Earth and Space Science

RESEARCH ARTICLE
10.1029/2019EA000567

Key Points:
- Permanently shadowed regions (PSRs) on flat floors of polar crater have systematically higher 1,064-nm albedo than the adjacent terrains
- Exposed surface water ice, not other factors, serves as the most plausible explanation for the elevated 1,064-nm albedo of these PSRs
- The inferred PSR water ice exposures are in very small quantity and laterally heterogeneous in model water ice abundance

Supporting Information:
- Supporting Information S1

Correspondence to:
L. Qiao and Z. Ling,
leqiao.geo@gmail.com;
zcling@sdu.edu.cn

Citation:
Qiao, L., Ling, Z., Head, J. W., Ivanov, M. A., & Liu, B. (2019). Analyses of Lunar Orbiter Laser Altimeter 1,064-nm albedo in permanently shadowed regions of polar crater flat floors: Implications for surface water ice occurrence and future in situ exploration. *Earth and Space Science*, *6*, 467–488. https://doi.org/10.1029/2019EA000567

Received 18 JAN 2019
Accepted 27 FEB 2019
Accepted article online 4 MAR 2019
Published online 22 MAR 2019

©2019. The Authors.
This is an open access article under the terms of the Creative Commons Attribution-NonCommercial-NoDerivs License, which permits use and distribution in any medium, provided the original work is properly cited, the use is non-commercial and no modifications or adaptations are made.

Analyses of Lunar Orbiter Laser Altimeter 1,064-nm Albedo in Permanently Shadowed Regions of Polar Crater Flat Floors: Implications for Surface Water Ice Occurrence and Future In Situ Exploration

Le Qiao[1], Zongcheng Ling[1], James W. Head[2], Mikhail A. Ivanov[3], and Bin Liu[4]

[1]Shandong Provincial Key Laboratory of Optical Astronomy and Solar-Terrestrial Environment, Institute of Space Sciences, Shandong University, Weihai, China, [2]Department of Earth, Environmental and Planetary Sciences, Brown University, Providence, RI, USA, [3]V. I. Vernadsky Institute of Geochemistry and Analytical Chemistry, Russian Academy of Sciences, Moscow, Russia, [4]State Key Laboratory of Remote Sensing Science, Institute of Remote Sensing and Digital Earth, Chinese Academy of Sciences, Beijing, China

Abstract Potential water ice concentrated within the permanently shadowed regions (PSRs) near lunar poles is both scientifically significant and of value for future explorations. However, after decades of observations, the existence and characteristics of PSR water ice remain controversial. The 1,064-nm laser reflectance measurements collected by the Lunar Orbiter Laser Altimeter (LOLA) onboard the Lunar Reconnaissance Orbiter (LRO) provide a unique opportunity to detect and characterize PSR water ice. In this work, we focus on all major PSRs on the flat floors of lunar polar craters and analyze their detailed LOLA 1,064-nm albedo and then compare this with the adjacent flat non-PSRs. We find that the LOLA albedo of the majority of these PSRs is systematically higher than their adjacent non-PSRs. Potential contributions of various factors to the observed LOLA albedo are individually quantitatively evaluated; we show that each of them is unable to account for the observed LOLA albedo anomalies and that the presence of surface water ice is the most likely explanation. Combined characterization of LOLA albedo and substrate impact cratering records (crater populations and depths) reveals that the inferred PSR water ices are in very small quantity (probably in the form of a surface frost layer or admixture with regolith) and are laterally heterogeneous in model ice concentration, ranging from negligible to ~6%. We recommend that these PSRs as priority targets for future surface in situ exploration endeavors, and a case assessment of Amundsen crater is presented.

Plain Language Summary The possible presence of surface water ice within the permanently shadowed regions (PSRs) in lunar polar areas is important for both science and future lunar resource exploration. However, significant uncertainty still exists concerning both the presence and properties of water ice in lunar PSRs. A recent Moon-orbiting laser instrument measures the laser brightness of the lunar surface, including areas that are permanently shadowed in visible light. These brightness data are very useful for studying the possible presence of water ice in PSRs, as water ice is much brighter than typical lunar surface soil. Our study finds that most of the PSRs on flat surface are generally brighter than the surrounding surface. We analyze many candidate reasons for this difference but find that the presence of water ice is the only explanation that can successfully explain the observations. We thus suggest that water ice very likely exists in many lunar PSRs. The surface water ice within PSRs is very thin and has different ice contents. These candidate ice-containing PSRs on flat surfaces are optimal landing sites for future lunar exploration and are an important reference base for future lunar mission site selection.

1. Introduction

The potential location and concentration of water ice and other volatile components on the Moon have tremendous significances for scientific studies of the solar system (e.g., planetary formation and evolution processes, source and migration history of water in the inner solar system, and water formation and evolution cycles on airless bodies), as well as for future robotic and human deep space exploration efforts (e.g., resources for rocket fuel and sustenance of human life). Due to the very low obliquity of the Moon relative to the ecliptic plane (1.54°), topographic depressions near the poles, mainly crater interiors, are permanently

shadowed from direct solar illumination (e.g., Mazarico et al., 2011; Speyerer & Robinson, 2013). Because the Moon's spin axis has been stable for billions of years (e.g., Siegler et al., 2015, 2016), these permanently shadowed regions (PSRs) can maintain extremely low temperatures, ranging from ~120 to 29 K (Paige et al., 2010), for geologically significant periods. Water components (in several forms) from a variety of sources (either endogenously released, exogenously delivered or generated in situ) that encounter such a cold surface would be potentially cold trapped within PSRs and accumulate there as water ice deposits due to very low evaporation rates (Watson et al., 1961; Zhang & Paige, 2009).

Because of their very special locations and environments (high latitude and not illuminated by the Sun), lunar polar PSRs and potential water ice are difficult to detect, measure, and study. Significant information about lunar PSR water has been gained in the half-century since the early Watson et al. (1961) contribution as outlined in the comprehensive summary of PSR water scientific exploration history and current knowledge of Lawrence (2017). Many fundamental aspects of lunar PSR water (its existence, distribution, and characteristics) are still not well understood, however. Prior investigations through various observational methods (orbital and Earth-based) covering a wide range of electromagnetic wavelengths (from gamma ray, optical to radio) have yielded controversial interpretations as to the existence and nature of water ice within lunar PSRs (see summary in Lawrence, 2017).

The Lunar Orbiter Laser Altimeter (LOLA), onboard National Aeronautics and Space Administration's Lunar Reconnaissance Orbiter (LRO) launched in 2009, is for the first time successfully conducting active (laser) reflectivity measurements of lunar PSRs at the near-infrared wavelength of 1,064-nm and zero-phase angle (Smith et al., 2010; Zuber et al., 2012). A decade of measurements have accumulated high spatial sampling 1,064-nm reflectance data for all major PSRs in both polar regions (Lemelin et al., 2016; Lucey et al., 2014); these data provide an unprecedented opportunity to detect and characterize surface water ice within lunar PSRs. Zuber et al. (2012) presented the first LOLA laser 1,064-nm reflectance measurements of one specific PSR within Shackleton crater at the south pole and found that the crater floor is more reflective than the surrounding terrain. Zuber et al. (2012) suggested the LOLA crater floor reflectivity anomaly could be primarily explained by decreased space weathering by micrometeorite bombardment, but a micrometer-thick surface layer containing 22% water ice served as an alternate possibility. Lucey et al. (2014) produced global LOLA 1,064-nm normal albedo maps of polar regions with 2-km spatial sampling size and found that polar PSRs are brighter than nonpermanently shadowed polar surfaces. They interpreted this elevated reflectivity as being due to either enhanced water frost (3–14 wt. % abundance) and/or an inefficient space weathering process; they found that medium porosity as a sole explanation can be largely ruled out. Fisher et al. (2017) carried out a combined analysis with LOLA albedo mapping and Diviner surface annual maximum temperature measurements and found a background trend of increasing albedo with decreasing temperature, which was interpreted to be due to a temperature-correlated space weathering effect. In particular, they observed a rapid increase of LOLA albedo below annual maximum temperatures of ~110 K near the south pole, a behavior consistent with the presence of persistent surface water ice deposits. They also found that the brightness anomalies of polar PSRs are mainly temperature dependent, not solar illumination correlated.

In summary, LOLA laser zero-phase angle reflectivity measurements provide a unique opportunity to investigate lunar PSR water ice. Previous LOLA reflectance data-based PSR ice detections are often subject to temperature and/or illumination-dependent space weathering effect uncertainties. Several prior studies have also tried to rule out the effects of topographic slopes and mass wasting on the observed LOLA reflectance through limiting analysis to areas with slopes <10° (Fisher et al., 2017; Lucey et al., 2014), while a systematic survey found that mass movement can proceed on gentle slopes (as small as ~5°; e.g., Xiao et al., 2013). Prior studies also commonly focused on the LOLA reflectivity characteristics of the entire PSRs or cold trap surfaces near poles (Fisher et al., 2017; Lucey et al., 2014), and thus, the interpreted surface water ice presence can be hampered by the heterogeneous nature of lunar polar crustal composition. From the perspective of lunar exploration, few PSR water ice detection and characterization studies using LOLA reflectance data have been dedicated to specific areas essential to future surface in situ exploration site selection and mission planning.

In this contribution, in order to examine the potential reflectivity anomalies of lunar PSRs and their spatial variations, we (1) target all major PSRs in the flat floors of lunar polar craters and characterize their detailed

LOLA 1,064-nm reflectivity and (2) compare these results with immediately adjacent non-PSR regions. Then, combined with other multisource data sets involving solar illumination conditions, surface temperature measurements, imaging spectroscopy, and long-exposure optical images, we quantitatively evaluate the potential effects and contributions of various nonwater ice factors on the observed LOLA reflectance, including illumination, temperature, surface composition variations and surface blockiness. Our goal is to achieve a more robust interpretation of the possible presence and characteristics of water ice in PSRs. Finally, we analyze the physical characteristics of surface water ice in representative PSRs, including water ice abundances and deposit thickness, through spectral unmixing modeling, and population and depth measurements of superposed impact craters. We also discuss the utility of our results for future surface in situ exploration missions and present an assessment of Amundsen crater as an optimal exploration target.

2. Strategy, Data, and Methodology

LOLA is a laser ranging instrument onboard National Aeronautics and Space Administration's LRO mission launched in 2009. LOLA has five beams that operate at 1,064-nm wavelength with a 28-Hz pulse repetition rate. From a 50-km altitude spacecraft orbit, each beam illuminates a 5-m-diameter spot ("data point") on the lunar surface. LOLA has an unprecedented vertical ranging precision of ~10 cm, making it an excellent tool for studying the surface topography and geologic processes of the Moon (Smith et al., 2010). During its many years of operation (Smith et al., 2017), as the LRO spacecraft orbits the Moon in a polar orbit, LOLA has accumulated the densest measurement coverage of the Moon in polar regions. The LOLA science team has used these comprehensive point measurements to construct high spatial sampling resolution digital elevation models (DEMs) for lunar polar regions, for instance, 20-m spatial resolution for polar regions extending to ±80° latitude (Smith et al., 2017). Mazarico et al. (2011) have employed these high-resolution LOLA DEMs to map the illumination conditions in polar regions during an 18.6-year lunar precession cycle and to document the distribution of lunar PSRs, which are in the subject of this work. We use these 20-m/pixel LOLA DEMs to study lunar PSR surface elevations and topographic slopes (with a baseline of 60 m) within the flat floors of lunar polar craters and the adjacent non-PSR regions. These high-resolution DEMs can also be used to generate shaded relief maps via simulating the illumination geometries (azimuth and altitude angles) in the ESRI ArcGIS platform. These synthetic high-resolution shaded relief maps can be particularly useful as surface images for geomorphological interpretation, crater identification and population studies (e.g., Tye et al., 2015; Zuber et al., 2012). Compared with typical optical images, these DEM-derived shaded relief maps have the unique advantage of varied illumination geometries, thus facilitating geomorphological interpretations and crater detections. We used these topographic products and shaded relief maps to study the impact crater populations and depths for polar PSRs and the adjacent non-PSRs. Our implementation of crater identification and diameter measurements is identical to typical crater counting studies (e.g., Fassett, 2016). The procedure of crater depth measurements includes the following steps: (1) a ring buffer area encircling the crater rim (±120 m in this work) is constructed, whose average elevation derived from the LOLA DEM is regarded as the average of the crater rim crest; (2) the minimum elevation of the crater interior is derived as the crater floor elevation; and (3) the difference between the average rim crest elevation and floor minimum elevation is calculated as the crater depth. As all of our craters studied are present in very flat regions, the effect of preexisting topography on the crater depth measurements should be insignificant.

In addition to surface altimetric measurements, LOLA has a "bonus" function that enables the mapping of reflectivity of the lunar surface through measuring the backscattered laser energy at the near-infrared wavelength of 1,064 nm. Using its own laser surface illumination source, LOLA has the unique ability to map lunar surface unilluminated by solar light (including lunar PSRs), providing an unprecedented opportunity to study the optical reflectivity of lunar polar PSRs. Moreover, LOLA can map the lunar surface reflectivity at zero-phase angles; this unique observational geometry can be very rarely achieved through typical passive optical measurements using solar illumination (including both Earth-based and orbital observations). Zero-phase angle reflectivity has been shown to be insensitive to local topographic relief (e.g., Hapke, 1993). We used the normal albedo measured by LOLA to characterize the optical reflectivity of lunar PSRs and compared these with the adjacent non-PSR areas. The processing, calibration procedures and acquisition of the LOLA albedo data is thoroughly documented in Lucey et al. (2014) and Lemelin et al. (2016). In this work, only the LOLA laser 1 raw, unsmoothed point measurements are employed for analysis, as laser 2 measurements have substantially higher uncertainties (Lemelin et al., 2016).

3. Results

3.1. LOLA 1,064-nm Albedo

We analyzed the LOLA zero-phase angle 1,064-nm albedo of each selected PSR and compared it with the albedo of the adjacent non-PSR (a "pair" of regions). Our search of PSR regions was based on the PSR distribution maps presented by Mazarico et al. (2011) and included PSRs larger than 10 km^2 in polar regions of latitudes poleward of ±80°. The selected region pairs are constrained to be within very flat regions (generally, slopes <~5°) on polar crater floors, with the goal of eliminating the slope effect of surface albedo and for the technical accessibility for surface spacecraft landing and in situ exploration. Our survey found 34 pairs of regions in 24 crater floors near the south pole (Figure 1a) and 41 pairs of regions in 29 crater floors near the north pole (Figure 1b). An example of regions selected for albedo analysis in Amundsen crater in the south polar region is shown in Figure 2. The surface area of the selected flat floor PSR and non-PSR regions ranges from ~1 to ~260 km^2, with a median and average value of 11.3 and 20.1 km^2 ($1\sigma = 33.5$), respectively, and the area difference between each analyzed PSR and the adjacent non-PSR is typically constrained to be within 10%. Although we found more flat floor PSRs in north polar region than in the south polar region, the north polar PSRs are much smaller in size (mean area of ~13.8 km^2) than south polar PSRs (mean area of 27.9 km^2); this is generally consistent with the results of PSR extent mapping by Mazarico et al. (2011), which shows the north polar region to host more micro-PSRs (<25 km^2). The average topographic slope of the floor areas studied is dominantly less than ~5°, with median and average values of 4.9° and 6.5° ($1\sigma = 4.2$), respectively, and the surface slope difference between each pair of regions are mostly less than 3°.

The LOLA 1,064-nm albedo of all the selected polar PSRs and their adjacent accompanying non-PSRs are plotted in Figure 3, with average values and one standard derivation (σ). Examination of Figure 3 shows that almost all (71 of 75) of the PSRs studied have higher 1,064-nm albedo values than their adjacent non-PSR areas. Null hypothesis tests are performed for several representative craters to show that the differences between the mean LOLA albedo of the floor PSRs is statistically different from that of the adjacent non-PSRs (Text S1 and Table S1 in the supporting information). The PSRs are on average ~5% (while they can be up to ~12%) more reflective than their adjacent non-PSRs; a very small portion ($n = 9$) of the PSRs studied are more than 10% brighter than their adjacent non-PSRs (Figure S1). In addition, the north polar region hosts more LOLA albedo anomalous PSRs than the south polar region, both in frequency and percentage (Figure S1), indicating that the distribution of LOLA albedo anomalous PSRs in the north polar region is more isolated.

3.2. Impact Crater Populations

Impact cratering is a ubiquitous geologic process operating continuously throughout the entire history of the Moon and having direct effects on almost all other lunar surface processes. In a similar manner, other surface processes may also affect the preserved impact cratering record (e.g., crater populations and depths, d) on the lunar surface. Therefore, it is essential to analyze the impact cratering record of lunar polar PSRs and to assess whether they show anomalies and how they compare with those of their adjacent non-PSRs. Due to the fact that surface topographic slopes have been shown to exert significant effects on preserved impact cratering records (e.g., Basilevsky, 1976; Qiao et al., 2018; Tye et al., 2015), we also confined our cratering record analyses to within very flat regions (predominantly <5° slope) of polar crater floors, similar to the LOLA albedo analysis above (section 3.1).

We used the 20-m/pixel LOLA shaded relief maps with varied illuminations to identify and measure impact craters in the PSR (the same area as for the LOLA albedo analysis in Figure 2) within the northern Amundsen crater flat floor (centered at 83.96°S, 91.57°E) in the south polar region (Figure 4a). We also analyzed craters within an adjacent non-PSR with the same surface area for a comparative crater counting study (with same area as the selected PSR, thus different from the non-PSR for albedo analysis; Figure 4a). The crater count analysis was completed for craters ≥200 m in diameter (D). We have taken particular care to eliminate contamination by secondary impact craters and nonimpact pits, according to their morphologic characteristics (e.g., Head & Wilson, 2017; Oberbeck & Morrison, 1974; Shoemaker, 1962). We identified 156 craters ≥200 m in diameter in the 96.5-km^2 PSR area and 257 craters ≥200 m in the adjacent, same-size non-PSR (Figure 4a and Table 1). The cumulative crater size-frequency distribution (SFD) plots (Figure 4b)

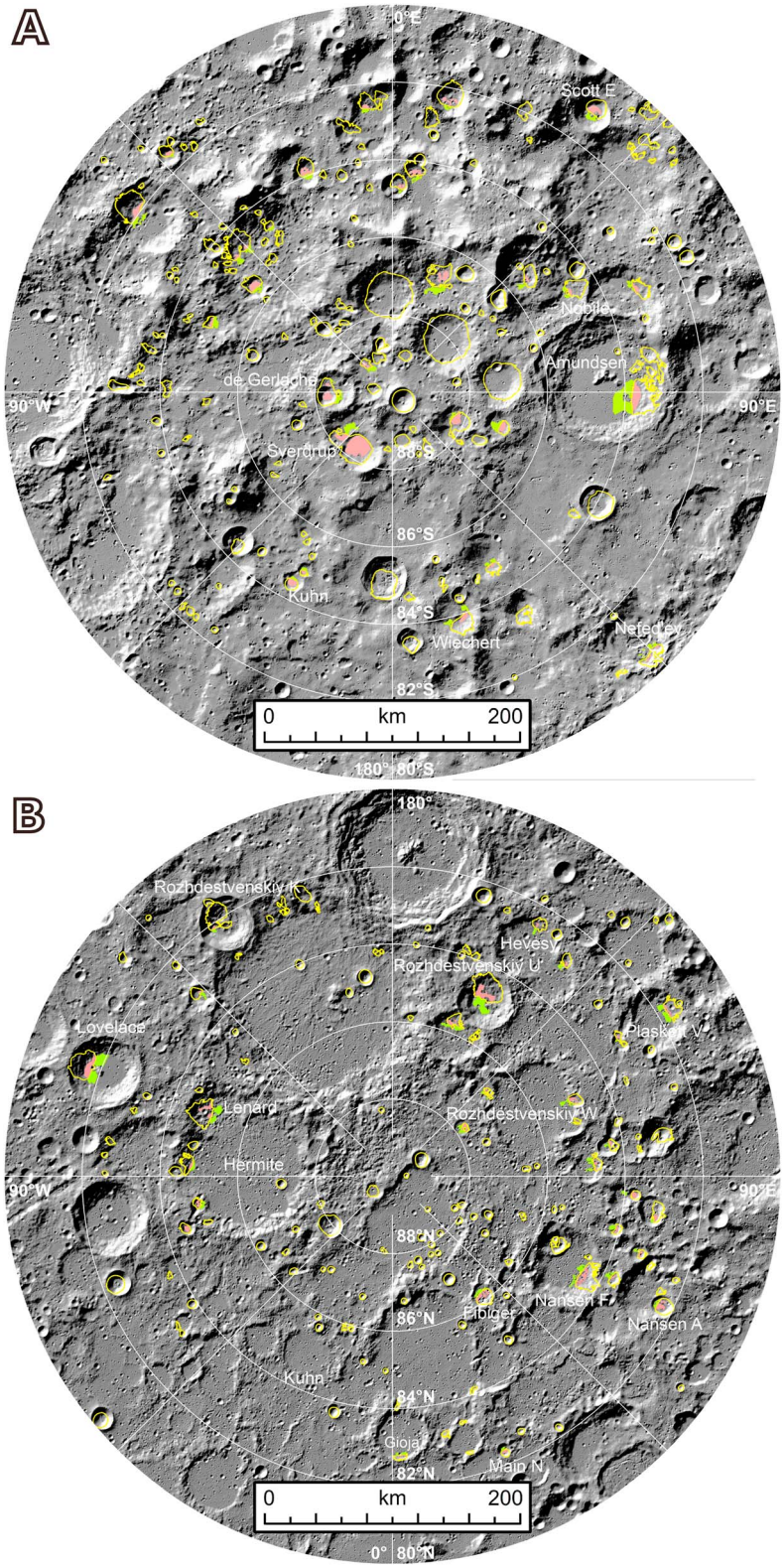


Figure 1. Distribution of the selected lunar permanently shadowed regions (PSRs; coral patches) and their accompanying adjacent non-PSRs (green patches) in the south (a) and north (b) polar crater flat floors, displayed on a shaded relief map (315° azimuth angle and 10° altitude angle). The distribution of PSRs larger than 10 km^2 from Mazarico et al. (2011) is denoted by yellow polygons. This map extends poleward of ±80° latitude, in polar stereographic projection (as do all other maps in this paper).

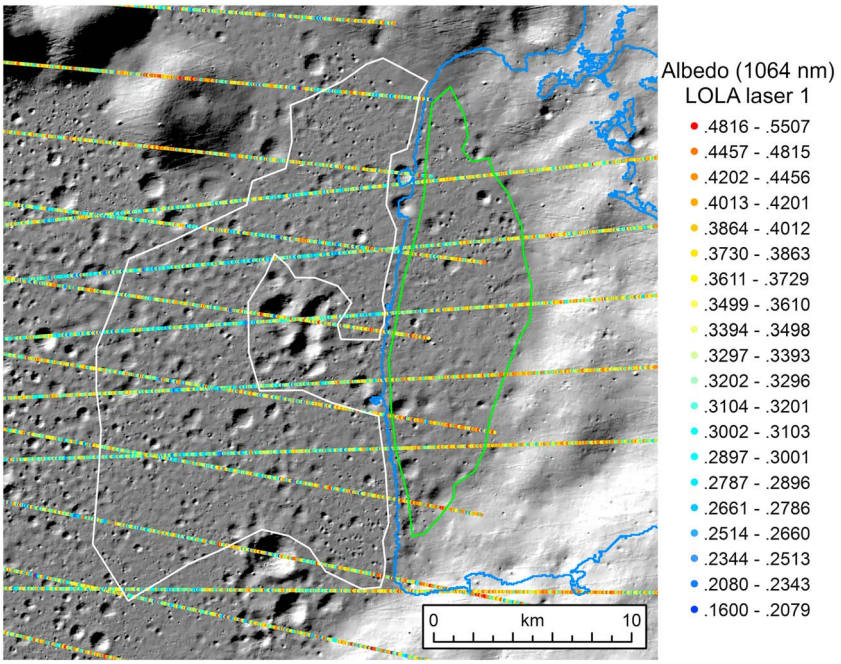


Figure 2. The selected PSR (green polygon) and the adjacent non-PSR (white polygon) within the northern floor of Amundsen crater (centered at 83.96°S, 91.57°E) selected for LOLA 1,064-nm albedo analysis (with data tracks overlain). The blue polygon marks the PSR coverage calculated by Mazarico et al. (2011). PSR = permanently shadowed region; LOLA = Lunar Orbiter Laser Altimeter.

show that the Amundsen PSR have a relatively decreased cumulative crater density at the <~800-m-diameter range than the adjacent non-PSR and for craters ≥800 m in diameter, the cumulative SFD of Amundsen PSR is indistinguishable from the adjacent non-PSR. Fitting of these PSR and non-PSR impact craters ≥800 m in diameter using the lunar chronology function (CF) and production function of Neukum et al. (2001) yields very close, pre-Nectarian absolute model ages (Figure 4b; $4.0^{+0.04}_{-0.06}$ Ga for the PSR and $4.0^{+0.04}_{-0.05}$ Ga for the non-PSR). We note, however, that although our crater counting results are robust, the specific crater population-derived pre-Nectarian model ages are particularly uncertain due to the poorly calibrated lunar CF beyond ~3.9 Ga.

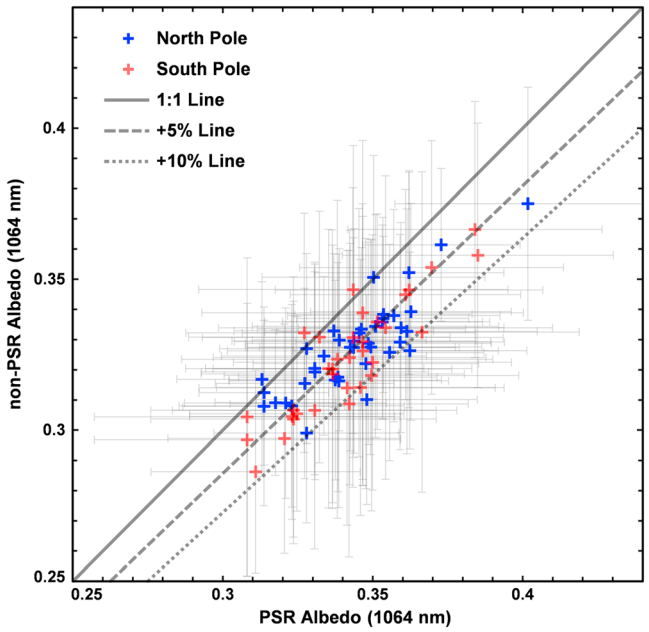


Figure 3. LOLA 1,064-nm albedo average values plus one standard deviation of the selected PSRs (horizontal axis) and the comparison with their adjacent non-PSRs (vertical axis). PSR = permanently shadowed region; LOLA = Lunar Orbiter Laser Altimeter.

We also performed impact crater population measurements on the PSR within the southern Nansen F crater flat floor (centered at 84.57°N, 62.54°E) in the north polar region (Figure 4c). An adjacent non-PSR with the same surface area and shape as the Nansen F floor PSR was also chosen for comparative crater counting analysis (Figure 4c and Table 1). Consequently, 136 impact craters ≥200 m in diameter were detected in the Nansen F floor 84.0-km^2 PSR area, and 162 craters ≥200 m were found in the adjacent non-PSR (Figure 4c). The cumulative SFD of the craters of the Nansen F PSR generally overlaps with that of the adjacent non-PSR for the entire diameter range (Figure 4d). Lunar CF fittings of craters ≥1 km in diameter also give very similar absolute model ages; $4.1^{+0.05}_{-0.07}$ Ga for PSR and $4.1^{+0.04}_{-0.06}$ Ga for non-PSR (Figure 4d).

3.3. Impact Crater Depths

In addition to impact crater populations, the depths of superposed impact craters in lunar PSRs may also be altered by potential subsequent surface

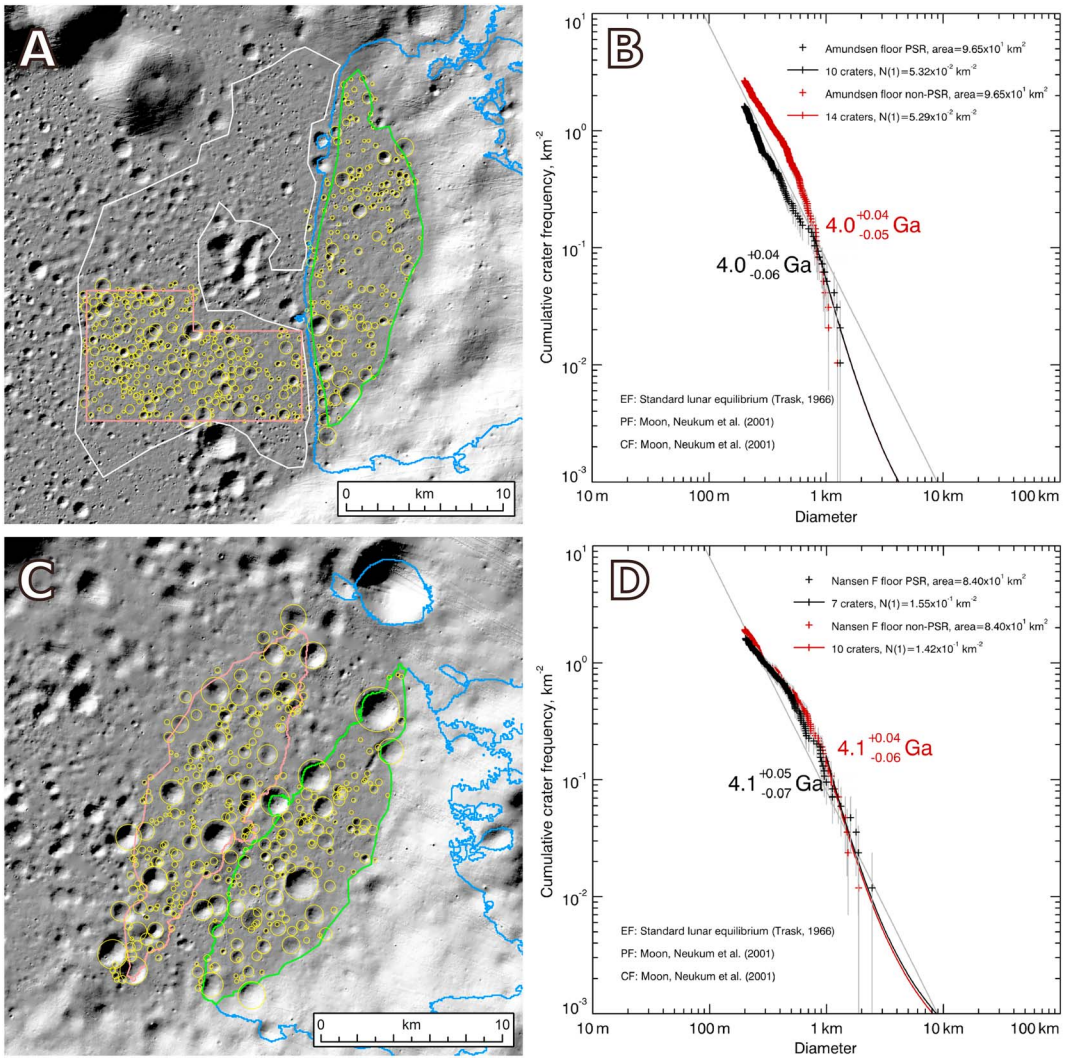


Figure 4. Superposed impact craters ≥200 m in diameter (with rim positions marked by yellow circles) identified in the permanently shadowed region (PSR; green polygon) and adjacent non-PSR (coral polygon) on the (a) northern Amundsen crater flat floor and (c) southern Nansen F crater floor. Cumulative size-frequency distribution of the impact craters counted on the (b) Amundsen and (d) Nansen F floor PSR (black crosses) and adjacent non-PSR (red crosses). The background images of panels A and C are Lunar Orbiter Laser Altimeter (LOLA) shaded relief maps (315° azimuth angle and 6° altitude angle), the blue polygons mark the PSR coverage (Mazarico et al., 2011) and the white polygon in panel A denotes the selected non-PSR for LOLA albedo analysis shown in Figure 2. The model age fitting is based on the production function (PF) and chronology function (CF) from Neukum et al. (2001), using the CraterStats software package (Michael et al., 2016; Michael & Neukum, 2010), and the gray line on the right is the lunar equilibrium function (EF) curve from Trask (1966).

Table 1
Numbers (#) of Superposed Impact Craters Identified in the PSR and the Adjacent Non-PSR on the Northern Amundsen Crater Floor and Southern Nansen F Crater Floor

Count area	Size of counting area (km^2)	# of craters D ≥200 m	# of craters D ≥500 m	# of craters D ≥1 km
Amundsen PSR	96.5	156	23	5
Amundsen non-PSR	96.5	257	51	3
Nansen F PSR	84.0	137	43	7
Nansen F non-PSR	84.0	162	47	10

Note. See Figures 4a and 4c for the study areas and full crater count maps. PSR = permanently shadowed region.

water ice depositing (e.g., Deutsch et al., 2018; Eke et al., 2017). Therefore, it is instructive to investigate the depths, specifically the depth-to-diameter ratios (d/D), of PSR craters and their comparison with those in adjacent non-PSRs. As a follow-up effort of our crater population analysis above (section 3.2), we conducted crater diameter and depth measurements for the northern Amundsen crater floor near the south pole (Figure 5a) and the southern Nansen F crater floor near the north pole (Figure 5b). The crater depth investigation is implemented for craters ≥800 m in diameter to ensure the LOLA altimetric measurements are sufficient to derive robust elevation values for crater rim crests and floors. The crater depth measurement results are plotted as d/D with respect to the crater diameter in Figures 5c and 5d. Examination of Figures 5c and 5d shows that PSR craters in both Amundsen and Nansen F floors have comparable d/D ratios with craters in adjacent non-PSRs for diameter ranges (0.8 to ~1.3 km). The Amundsen floor craters (in both PSR and non-PSR) have relatively clustered d/D values (dominantly between ~0.02 and 0.07) relative to the Nansen F floor craters (ranging from ~0.014–0.23).

4. Factors for Elevated LOLA 1,064-nm Albedo

Our LOLA zero-phase angle 1,064-nm albedo analysis shows unequivocally that the PSRs studied in both polar regions are predominantly more reflective than their adjacent non-PSRs, consistent with previous analyses (Fisher et al., 2017; Lucey et al., 2014). The similarly enhanced LOLA reflectance observed at the Shackleton crater floor PSR near the south pole has been suggested to be a possible indicator of a surface frost layer containing ~20% water ice, but a dearth of space weathering due to shadowing was cited as a more likely explanation (Zuber et al., 2012). We suggest in addition that the exposure of less mature materials via downslope mass movements on the steeper slopes (up to ~25°) of the floor mounds (observed in both Kaguya Terrain Camera images, Haruyama et al., 2008; and LOLA topography maps, Zuber et al., 2012) within Shackleton crater may also contribute to the observed elevated brightness.

Though our LOLA albedo analysis of lunar polar PSRs characterized by very flat surfaces (<5° slope) has largely eliminated brightness effects from steep slopes, the possible contribution to elevated albedo from decreased space weathering due to a lack of solar illumination should be separately evaluated from the contribution of the interpreted surface water ice deposits. Moreover, various additional nonwater ice factors may also contribute to or affect the observed elevated LOLA zero-phase angle 1,064-nm albedo, including surface composition variations, surface temperature, surface block exposure, etc. The potential effects of these factors are now quantitatively assessed so that a more robust interpretation of surface water ice presence can be formulated.

4.1. Solar Illumination

The most prominent characteristic of lunar PSRs is their permanent shielding from solar illumination by surrounding topographic features, so it is of great interest to explore whether or not the solar illumination received has a significant effect on the measured LOLA albedo of the lunar surface. The relatively enhanced reflectance of the Shackleton crater floor PSR has been interpreted as weakened space weathering due to shadowing and/or surface water ice exposure (Zuber et al., 2012), but it is unclear how the former factor compares with the latter in importance. In general, the longer a specific lunar surface has been exposed to the harsh space environment, the more enhanced space weathering it would have experienced, thus becoming optically more mature and lower albedo (e.g., Pieters & Noble, 2016). While one of the primary agents of lunar space weathering, solar wind, is not expected to follow the exact travel path of solar illumination, a less illuminated lunar surface will tend to receive less solar wind implantation than an adjacent more illuminated surface (e.g., "solar wind orographic effects"; Farrell et al., 2010). As the other space weathering agents, that is, micrometeorite bombardment and cosmic rays, are not genetically related to solar illumination, it seems reasonable to assume that these agents would not show significant differences between variably illuminated lunar surfaces, when keeping other parameters unchanged, including topographic elevations and absolute surface model ages (section 3.2). We here first analyze the potential effect of solar illumination on lunar surface LOLA albedo measurements.

We selected four representative polar craters (two in the south polar region: Amundsen and Cabeus B; two in the north polar region: Nansen F and Lovelace) with relatively extensive floors which contain both PSRs and non-PSRs with diverse illumination conditions (average illumination time during a lunar precession cycle; Mazarico et al., 2011). Several patchy areas with incremental time-weighted illumination conditions are

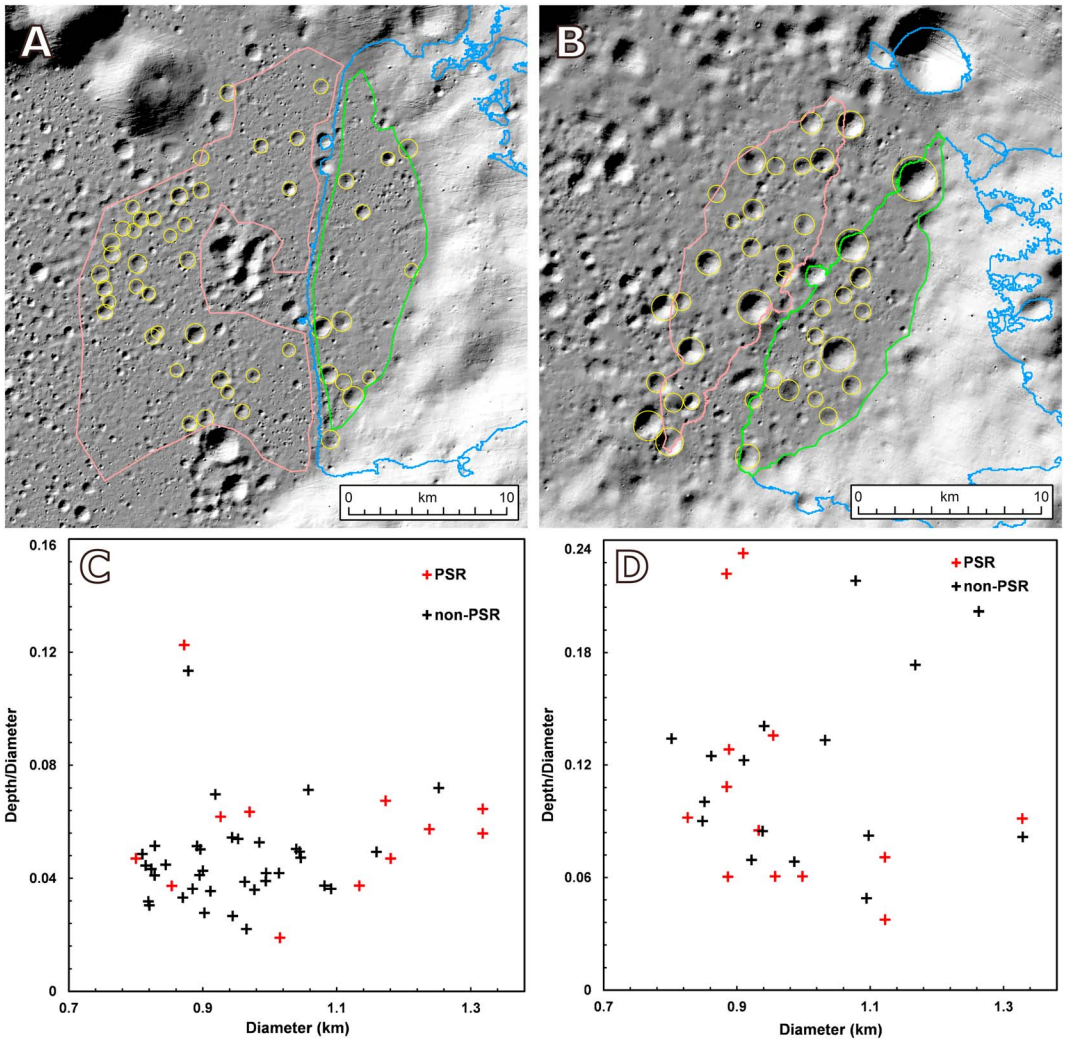


Figure 5. Distribution of impact craters (with rim positions marked by yellow circles) in the permanently shadowed regions (PSRs; green polygons) and adjacent non-PSRs (coral polygons) for the crater depth analysis: (a) the northern Amundsen crater floor and (b) the southern Nansen F crater floor. The blue polygons denote the extent of PSRs. Variations in depth-to-diameter ratios with respect to diameters of measured impact craters in (c) Amundsen and (d) Nansen F floor PSR (red crosses) and non-PSRs (black crosses).

delineated to characterize their LOLA 1,064-nm albedo (see Figure 6a as an example at the Amundsen crater floor). To eliminate the effect of topographic relief and immature material exposure, relatively fresh craters with steep interior walls are excluded from the analysis areas. The plots of LOLA albedo (mean value $\pm 1\sigma$) with respect to illumination condition (also mean value $\pm 1\sigma$) show clearly that, for all the four studied polar craters, the floor PSRs are apparently more reflective at 1,064 nm than their adjacent non-PSRs and that the floor non-PSRs with variable illumination conditions generally have almost identical 1,064-nm albedo values (Figure 7a). The latter observation shows unequivocally that solar illumination itself, and its potentially related influence on space weathering, has no obvious (or negligible) effect on the observed 1,064-nm surface albedo. Null hypothesis tests have been implemented for the craters studied and show that the LOLA albedo differences between the PSRs and the non-PSRs within the same crater floor are statistically significant (Text S1 and Table S2).

4.2. Surface Temperature

Extremely cold temperature (as low as ~30 K; Paige et al., 2010) is another special physical property of lunar PSRs; as a consequence, water and other volatile components can be cold trapped and remain stable there for geologically long time periods. Previous studies have suggested that surface temperature was one of the most

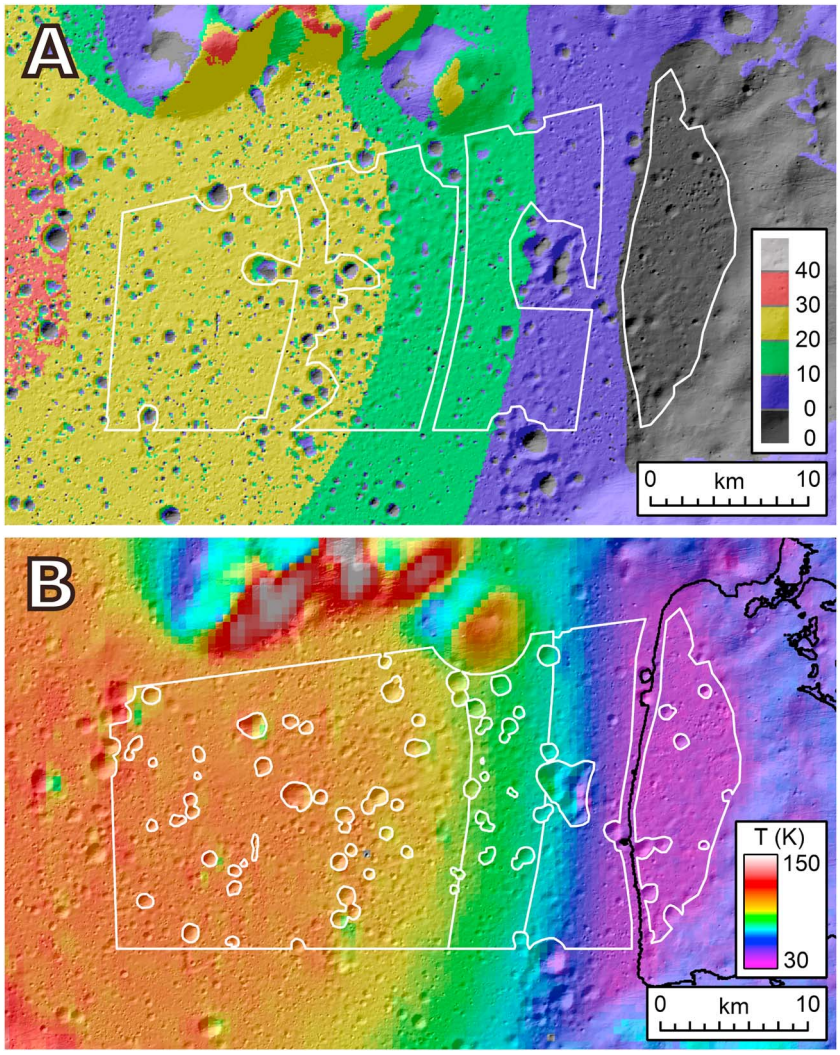


Figure 6. (a) Colorized time-weighted illumination condition (average illumination time during a lunar precession cycle, in percent) and (b) Lunar Reconnaissance Orbiter Diviner-measured annual average bolometric brightness temperature (*T*) maps of the northern Amundsen crater floor, overlain on a shaded relief map. The several patchy areas in each panel, including a PSR at the right of each panel, for (a) illumination condition and (b) surface temperature-albedo analyses (Figure 7) are outlined with white polygons; black polygon in panel (b) marks the extent of PSRs.

important and key factors controlling the deposition and preservation of lunar surface water ice (e.g., Lucey et al., 2014; Zhang & Paige, 2009). Cold temperatures at lunar PSRs may also inhibit the mechanical disruption of lunar boulders and space weathering of surface materials, which further retard the darkening of the lunar surface. Laboratory experiments have shown that low temperatures can indeed weaken the space weathering process, while the resultant surface brightness changes depend on the chemical composition of the substrate materials: For typical iron-bearing minerals (e.g., olivine and pyroxene), space weathering at low temperatures can lead to an ~5% brightening at 1,064 nm compared to that at ambient temperature, but for iron-depleted materials (e.g., feldspathic lunar polar regions), weathering at different temperatures does not induce measurable surface reflectivity difference at 1,064 nm, even when the duration of the simulated space weathering process has been prolonged (Corley et al., 2016, 2017). Therefore, the potential effect of surface temperature on the LOLA 1,064-nm measured albedo should be evaluated before a definitive conclusion on the presence of surface water ice can be made.

Annual average bolometric brightness temperatures measured by the LRO Diviner infrared radiometer (Level 4 Polar Resource Products) are employed for the surface temperature-surface albedo analysis of

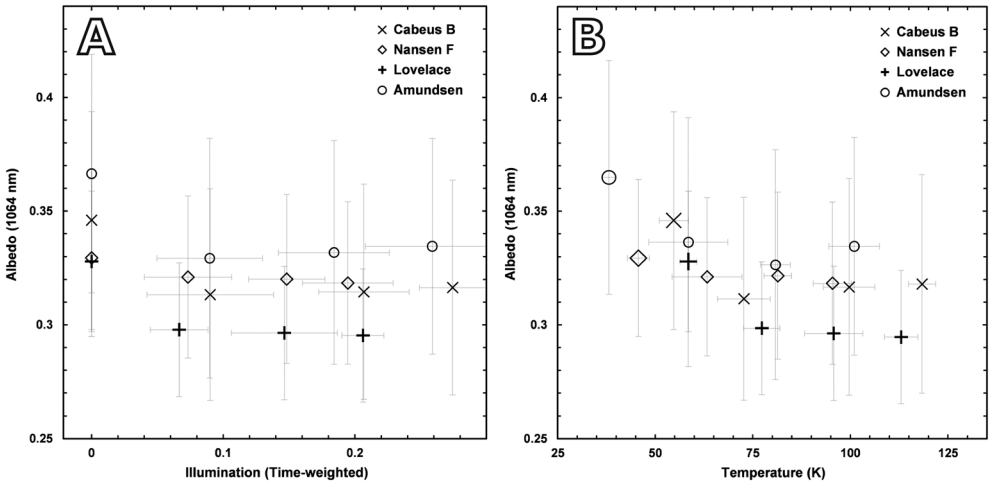


Figure 7. Plots of Lunar Orbiter Laser Altimeter 1,064-nm albedo with respect to (a) illumination condition and (b) annual average surface temperature (all plotted as mean value $\pm 1\sigma$) of the selected floor areas in four polar craters (see Figure 6, Amundsen crater, as an example). In each panel, the leftmost data point (lowest illumination condition or temperature) of each crater floor is that of the floor permanently shadowed region (larger point markers).

lunar polar PSR-hosting crater flat floors. These temperature data are calculated from the first year of Diviner thermal mapping of lunar polar regions, at a spatial sampling size of ~500 m (Paige et al., 2010). As we focus here on the potential effects of cold surface temperatures on the postemplacement modification of lunar surface materials (which should be regarded as a continuous processes and whose resultant effects should be cumulative), we adopt the annual average surface temperature, rather than the annual maximum temperature used in previous works assessing the thermal stability of surface water ice (e.g., Fisher et al., 2017; Hayne et al., 2015). Patchy surface areas with a wide range of annual average surface temperatures on the floors of several representative polar craters were selected, whose average LOLA 1,064-nm albedo and Diviner surface temperatures were calculated (see Figure 6b as an example of the Amundsen crater floor). Examination of the surface albedo-temperature plots shows that the 1,064-nm surface albedo indeed varies along with the annual average surface temperature, and a general trend (on three of the four studied crater floors) is an increased surface albedo with lower surface temperature (Figure 7b), plausibly indicating diminished space weathering and/or mechanical disruption at lower temperatures. At the Lovelace crater floor, for instance, an ~18-K temperature decrease at non-PSRs approximately indicates an ~1% surface brightening, consistent with laboratory studies (e.g., Corley et al., 2016). The PSRs are all well beyond the albedo-temperature trend line of their adjacent non-PSRs and are characterized by a significantly elevated surface albedo, for example, over ~10% more reflective of the Lovelace PSR relative to the adjacent non-PSR floors. Null hypothesis tests have also been implemented for these studied craters to show that the LOLA albedo differences between the PSRs and the non-PSRs with variable surface temperatures within the same crater floor are statistically significant (Text S1 and Table S3). We thus conclude that the surface temperatures may affect, but to a very slight degree, the LOLA 1,064-nm albedo measured, and additional factors other than surface temperatures are required to explain the elevated albedo of lunar polar PSRs. The observed rapid albedo increases of PSRs compared with the immediately adjacent non-PSRs are consistent with the reflectivity-behavior of the presence of surface water ice (e.g., Fisher et al., 2017; Schorghofer & Taylor, 2007; Zhang & Paige, 2009).

4.3. Surface Composition

Variation in surface composition is another major factor that has significant effects on lunar surface reflectivity (for example, the apparent brightness difference between lunar mafic mare and feldspathic highlands). A compositional anomaly (presence of naturally high-reflectance purest anorthosite, PAN) observed by the Kaguya Multi-band Imager (MI) has also been suggested as an alternative explanation for the elevated brightness of the Shackleton floor (Haruyama et al., 2013). Moreover, for prior LOLA reflectance data-based lunar PSR water ice detections generally aimed at the entire polar regions (e.g., Fisher et al., 2017; Lucey

et al., 2014), it is unknown whether the conclusions are influenced by surface compositional variations, as the lunar high-latitude and polar crustal regions have been shown to be highly heterogeneous in surface composition from both lateral and vertical perspectives (e.g., Cahill et al., 2009; Ohtake et al., 2012) and sporadically host bright anorthosite-rich lithologies (e.g., Donaldson Hanna et al., 2014; Yamamoto et al., 2012). Therefore, it is crucial to examine the surface composition of the polar crater floors as part of our analysis and interpretation of our LOLA albedo (section 3.1).

We employed the Kaguya MI reflectance data (Ohtake et al., 2008; MAP level) of lunar polar regions (up to ±85° latitude) to investigate the surface composition of the eastern Amundsen crater floor (Figure 8). While the MI instrument is not sensitive enough to map the unilluminated surfaces (including PSRs), its reflectance measurements at multiple visual and near-infrared bands can reveal the surface composition and its potential variations in the adjacent illuminated regions (non-PSRs), which serve as an indicator of the surface composition variations of the unmapped PSRs. The 1,050-nm reflectance map (Figure 8a) shows that the eastern crater floor is relatively uniform in surface reflectance, predominantly ranging between ~0.15 and 0.3 and that most of the enhanced reflectance distributions are associated with the steep walls of small impact craters and areas adjacent to shadowed regions, suggesting that these reflectance anomalies are mainly caused by unweathered material exposures and/or improper calibration of the MI data, rather than a real reflection of local surface compositional variations. The map of the 1,050/1,250-nm reflectance ratio (Figure 8b), as a measurement of the diagnostic 1,250-nm absorption band of PAN, also reveals that the eastern Amundsen floor is relatively homogeneous in surface composition and that no clear PAN occurrences are observed. Some stripe-shaped areas (indicated by the white arrow in Figure 8b) close to the shadowed region are characterized by an increased 1,050/1,250-nm ratio and a plausible 1,250-nm spectral absorption feature. But we undertook a cross check of these areas on the reflectance map (Figure 8a), and this shows that they have abnormally low reflectance (mostly <0.01), inconsistent with the presence of high-reflectance PAN. We thus conclude that these high 1,050/1,250-nm ratio areas are again caused by the data quality issue. Although the MI spectrometer cannot directly measure the surface composition of the Amundsen floor PSR, it is plausible to predict that the PSR may have a relatively uniform surface composition together with the adjacent non-PSR floor when they were emplaced during crater formation. In summary, we suggest that the elevated 1,064-nm albedo observed at the lunar polar flat PSRs cannot be readily explained by local surface compositional anomalies.

4.4. Surface Block Exposure

Potential surface block exposures are another major obstacle to the definitive interpretation of the presence or absence of surface water ice in lunar polar PSRs, since blocky materials can exert comparable effects to the observed surface reflectivity (increased reflectivity due to exposure of less weathered blocky materials) and radar scatter signals (e.g., coherent opposition backscatter effect, enhanced radar backscatter, circular-polarization ratio [CPR] value and *m-chi* parameter; Fa & Cai, 2013; Hapke, 1990; Raney et al., 2012). As LOLA measures the reflectivity of the uppermost micrometer layer of the lunar surface directly, it is of great interest to examine the occurrence, size and population of surface blocks on lunar PSRs and their comparison with the adjacent non-PSRs. While permanent shielding from direct solar illumination prevents regular optical imaging of the PSR surfaces, high-sensitivity cameras, through elaborate operations during lunar summer solstices, can directly map the PSRs occasionally illuminated by secondary lighting scattered from nearby higher terrains, including crater walls and massifs (Haruyama et al., 2008; Koeber & Robinson, 2013). The Lunar Reconnaissance Orbiter Camera (LROC) Narrow Angle Cameras (NAC) has obtained a comprehensive image data set for many major lunar PSRs during its multiple long-exposure imaging campaigns (Cisneros et al., 2017; http://lroc.sese.asu.edu/psr). The required prolonged exposure times (~10–20 ms vs. the <~2-ms nominal case) for imaging weakly lit surfaces result in considerable along-track smear and thus a one-magnitude decrease in image spatial resolution (~10–40 m/pixel vs. the typical 0.5–2 m/pixel). From these long-exposure NAC frames, blocks larger than ~20 m can be identified and measured (a minimum size of two pixels). An example of such a long-exposure NAC image mosaic of the southern floor of Lovelace crater (centered at 81.68°N, 110.16°W) in the norther polar region is shown in Figure 9. Examination of NAC images of PSRs on the Lovelace floor and elsewhere, and their adjacent non-PSRs, shows no obvious surface texture disparities between the PSRs studied and their adjacent non-PSRs. In addition, very few to no blocks larger than 20 m are identified in these PSRs, indicating that the PSRs are not characterized by elevated

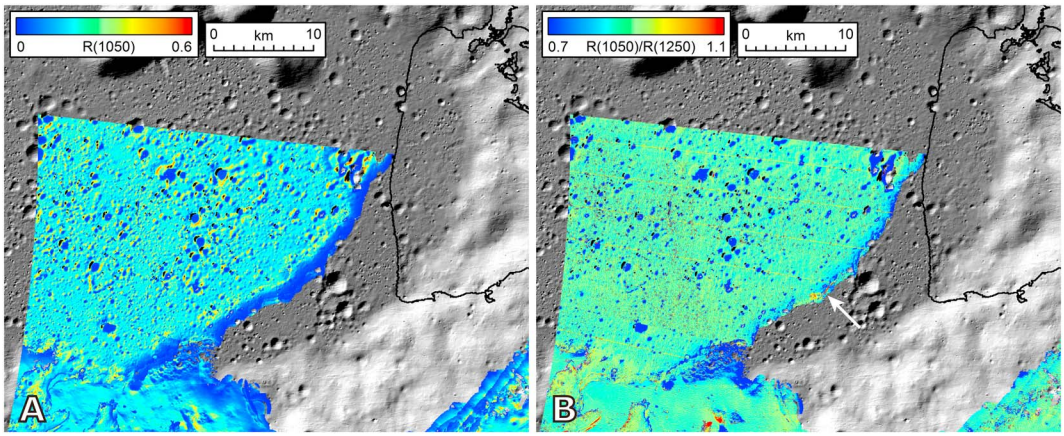


Figure 8. (a) The 1,050-nm reflectance (R(1,050)) and (b) 1,050/1,250-nm reflectance ratio (R(1,050)/R(1,250)) maps of the eastern Amundsen crater floor, generated from Kaguya Multi-band Imager mosaic data. The background image is a Lunar Orbiter Laser Altimeter shaded relief map (315° azimuth angle and 10° altitude angle), the white arrow in panel b indicates stripe-shaped areas of enhanced 1,050/1,250-nm ratios, and the black polygons mark the extent of permanently shadowed regions.

abundance of large blocks (consistent with the results of Mitchell et al., 2017). However, this documentation of the large boulder population cannot necessarily lead to the conclusion that the PSRs are not blockier than their adjacent non-PSR, as giant blocks larger than ~20 m are extremely rare on the lunar surface (e.g., Basilevsky et al., 2013; Krishna & Kumar, 2016).

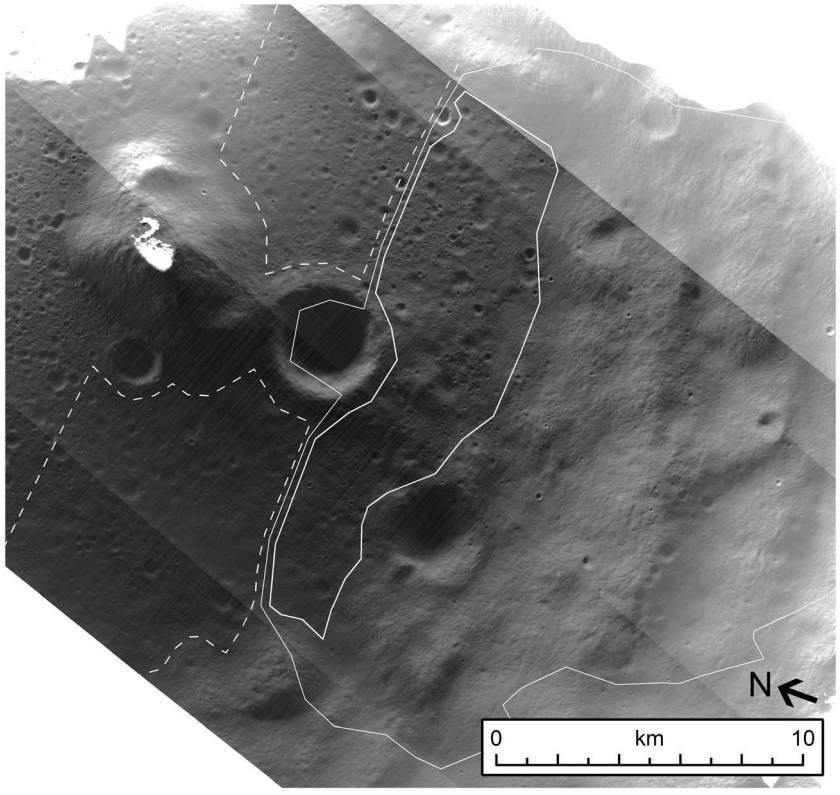


Figure 9. Lunar Reconnaissance Orbiter Camera Narrow Angle Cameras (NAC) long-exposure image of the northern floor of Lovelace crater (centered at 81.68°N, 110.16°W, a portion of NAC mosaic NAC_ROI_PSRLOVELLOA_P814N2503) in the north polar region. The polygons outlined by bolder white line and dashed white line denote the selected permanently shadowed region (PSR) and adjacent non-PSR, respectively, for Lunar Orbiter Laser Altimeter albedo analysis (Figure 1b), and the polygon outlined by the thinner line marks the PSR extent calculated by Mazarico et al. (2011).

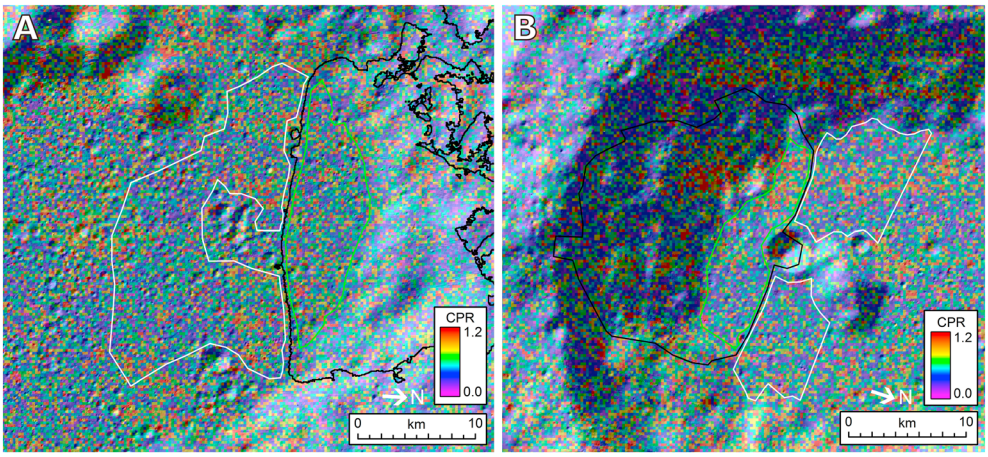


Figure 10. Mini-RF S band circular-polarization ratio (CPR) maps of (a) the southern Amundsen crater floor (centered at 83.92°S, 91.32°E) and (b) the southern Lovelace crater floor (centered at 81.65°N, 110.18°W). The polygons outlined by the green line and white line denote the selected permanently shadowed region (PSR) and adjacent non-PSR, respectively, for Lunar Orbiter Laser Altimeter albedo analysis (Figure 1), and the polygon outlined by the black line marks the PSR extent calculated by Mazarico et al. (2011).

To further characterize the presence and distribution of surface blocks at ranges of smaller dimension, we alternatively utilize the Mini-RF S band 12.6-cm CPR map (Nozette et al., 2010; Level 3 Derived Global Mosaic Data Record) to analyze the physical properties of lunar PSRs. This data product is particularly sensitive to surface and shallow subsurface (to a maximum depth of 10 times the radar wavelength, that is, ~1 m) blocks larger than ~0.3 m (three radar wavelengths). Portions of such Mini-RF CPR mosaic images of the Amundsen crater floor near the south pole and the Lovelace floor near the north pole (Figure 10) demonstrate that the PSRs studied generally have indistinguishable CPR values compared to their adjacent non-PSRs. The mean CPR values for the selected PSR and adjacent non-PSR are very close: 0.62 ± 0.55 versus 0.61 ± 0.64 on the Amundsen floor; 0.58 ± 0.35 versus 0.60 ± 0.84 on the Lovelace floor. PSRs on both the Amundsen and Lovelace crater floors are ~10% more reflective at 1,064 nm than their adjacent non-PSRs. This analysis indicates that crater flat floor PSRs are not characterized by higher surface rock abundance relative to their accompanying adjacent non-PSRs; thus, their elevated LOLA 1,064-nm albedos call for an additional explanation, other than surface block exposures. Furthermore, the lack of observed enhanced and greater-than-unity CPR values also preclude the existence of thick surface water ice deposits, consistent with prior observations (e.g., Campbell et al., 2006).

5. Constraints on Surface Water Ice Occurrence

5.1. Evidence for Surface Water Ice Exposure

Our detailed LOLA 1,064-nm albedo analysis of the many PSRs on lunar polar crater flat floors demonstrates clearly that these PSRs are symmetrically more reflective than their adjacent non-PSRs. Prior LOLA albedo data-based surface water ice detections (e.g., Lucey et al., 2014; Zuber et al., 2012) are usually subject to the possible effect of potentially decreased space weathering in PSRs (largely due to shadowing). Space weathering is generally thought to proceed when surface materials on airless bodies are exposed to the harsh space environment, including interplanetary dust and micrometeorite bombardment, solar and cosmic ray irradiation, and solar wind implantation and sputtering (e.g., Pieters & Noble, 2016). On the lunar surface, an excellent representative of space environment at 1 AU, solar wind flux is arguably the most dominant agent of the space weathering process (e.g., Hemingway et al., 2015; Sim et al., 2017). In the same manner as with solar illumination, the distribution of solar wind flux on the lunar surface is also obstructed by topographic features; thus, lunar surface solar illumination conditions tend to correlate with the solar wind flux received (Farrell et al., 2010; Feldman et al., 2001). Our detailed comparative analysis of the relationship between surface albedo and solar illumination conditions of PSRs and adjacent non-PSRs (section 4.1) shows that the received solar wind flux variations and their potential related effect on space weathering process

cannot solely explain the apparently elevated 1,064-nm albedo of the polar PSRs studied. Another major space weathering agent, micrometeorite bombardment, has also been demonstrated to not be an explanation for the observed 1,064-nm albedo difference between lunar polar PSRs and non-PSRs (via space exposure analysis; Lucey et al., 2014). Our evaluations of other nonwater ice factors, including solar illumination, surface temperature, surface composition variations, surface boulder exposure, topographic slopes and their related effects on space weathering, physical disruption, and mass motion, all find that each of them cannot account for the observed apparent LOLA albedo discrepancy. As a consequence of ruling these out as major contribution factors, we suggest that the specific reflectance behaviors of lunar polar crater flat floor PSRs and their comparisons with immediately adjacent non-PSRs can be best explained by the possible presence of surface water ice within these studied PSRs.

In addition, other volatile species, including sulfur-bearing species, carbon dioxide, and hydrocarbons, have been demonstrated to be stable in lunar PSRs (Zhang & Paige, 2009) and were detected in the Lunar Crater Observation and Sensing Satellite (LCROSS) impact ejecta plume (Colaprete et al., 2010; Schultz et al., 2010). These volatiles may also contribute, in part, to the elevated LOLA albedo of lunar PSRs. However, spectral measurements from the LCROSS experiment also show other nonwater volatiles are much lower in abundance (at least 1 order of magnitude lower) compared to water ice (Colaprete et al., 2010). We conclude that water ice still appears to be the major explanation for the elevated LOLA albedo of the many investigated lunar PSRs.

5.2. Characterization of Polar Water Ice Exposures and Deposits

In addition to presenting the evidence of surface water ice exposure in the PSRs of polar crater flat floors, our integrated investigations of the surface 1,064-nm albedo and the impact cratering record also provide an insight into the nature of the inferred polar surface water ice. LOLA is only able to sample the uppermost micrometer of the surface, and radar echo experiments do not positively indicate the presence of thick surface water ice deposits (section 4.4); the interpreted water ice materials may be in the form of a surface frost layer or an admixture of water ice particles within the regolith of the PSRs. This interpretation is also supported by our crater population and depth investigations, which show that surface water ice deposition in polar PSRs is not voluminous enough to modify the superposed cratering record (sections 3.2 and 3.3). The interpreted very small quantity of lunar PSR water ice suggests that the retention of surface water ice materials at lunar polar regions may be a dynamic process, for instance, volcanically erupted water migrating toward the poles and cold trapped in PSRs, and then being subject to sublimation due to impact gardening (Hayne et al., 2015; Needham & Kring, 2017).

Our exhaustive survey of the 1,064-nm albedo of all major PSRs on lunar polar crater flat floors shows the vast majority of these PSRs are characterized by elevated LOLA 1,064-nm albedo, suggesting surface water ice exposure may be a prevalent phenomenon in lunar polar cold traps. In addition, the albedo anomalies of each individual PSRs (compared with their adjacent non-PSRs) vary from negligible to over 10% more reflective, indicating that the inferred surface exposed water ice occurrences are laterally heterogeneous in model ice abundance. We adopt a simple linear albedo mixing model based on the assumptions that (1) the adjacent non-PSR studied is water ice-free and the elevated albedo measurements for most of the PSRs are solely attributed to surface water ice presence, (2) the water ice on the PSR surfaces is pure while patchily mixed with the background materials (lunar regolith, with composition assumed to be comparable with the adjacent non-PSRs) at the subpixel level, and (3) the surface water ice layer (or frost) has an apparently high albedo of 0.9 (Antarctic sea ice covered by a ~1 cm of snow; Brandt et al., 2005). Our unmixing calculations show that these analyzed PSRs are characterized by a heterogeneous inferred model water ice abundance, ranging from almost ice free to up to ~6% by surface area. For instance, the PSR at the norther marginal floor of Cabeus crater in the south polar region, which has been impacted and observed by the LCROSS mission, is ~5% more reflective than the adjacent non-PSRs, corresponding to an inferred model water ice content of ~3%. Adapting an intimate mixing model (linearized by mixing single scattering albedos) and considering the effect of porosity on near-infrared reflectance (assuming a porosity of 70%) would produce a slightly higher water ice content, for example, ~6.5% for the LCROSS impact site, generally consistent with the detection value for the ejecta plume from the Cabeus crater floor (5.6 $\pm$ 2.9%; Colaprete et al., 2010). Recent M^3 spectroscopic modeling calculations for lunar polar PSRs by Li et al. (2018) also revealed a higher water ice abundance from intimate mixing modeling than areal mixing modeling. Our investigation also shows

that the north polar region hosts more smaller and LOLA albedo anomalous PSRs than in the south polar area, indicating the distribution of surface water ice exposure is more isolated in north polar region than in the south polar region, consistent with previous studies (e.g., Fisher et al., 2017; Gladstone et al., 2012; Li et al., 2018). The highly heterogeneous spatial distribution of surface water ice content in lunar polar regions may indicate different water delivery flux, water ice loss mechanisms and rates, and local thermal environment variations.

5.3. Implications for Future Investigations

We have attempted to be exhaustive in our analysis of the factors contributing to LOLA albedo differences (section 4.1) and surface water ice detection and characterization (sections 5.1 and 5.2); there are still some additional factors that need to be analyzed and clarified before the presence and nature of surface water ice in PSRs can be determined confidently. (1) Surface materials within lunar PSRs have been suggested to be much more porous than the adjacent non-PSRs (e.g., Gladstone et al., 2012; Hayne et al., 2010; Schultz et al., 2010). Medium porosity has long been known to have fundamental and convoluted effects on surface reflectivity measurements. A prevalent, simple trend is the decreasing of reflectivity with increased porosity; considering this simplified porosity-reflectivity relationship would result in a higher estimated water ice content for lunar PSRs (e.g., the estimation for Cabeus crater floor PSR in section 5.2). However, this porosity dependence has been shown to be complicated by other factors, including medium albedo (e.g., Hapke, 2008), and thus, additional detailed and quantitative analyses on the effects of medium porosity on the PSR 1,064-nm albedo are required in future investigations. (2) The extreme low temperatures at lunar PSRs might retard the mechanical disruption of lunar surface boulders, which could potentially result in enhanced surface boulder exposure and thus elevated surface reflectivity. Currently available optical imaging data, however, are only able to identify very large surface boulders (>20 m in dimensions), and thus, the vast majority of surface boulders cannot be directly resolved. Advanced imaging operations and/or specifically dedicated cameras are required to provide high-resolution (meter scale) images of the surface of lunar PSRs. For instance, the ShadowCam to fly on the forthcoming Korea Pathfinder Lunar Orbiter would provide an excellent opportunity to obtain these data (Robinson et al., 2017; http://shadowcam.sese.asu.edu). (3) The very cold PSR environment would also introduce special physical (mechanical, rheological, etc.) properties for the inferred water ice components and their interaction with PSR regolith, which are, however, not well understood. How these factors might modify the LOLA reflectivity measurements needs to be specifically explored in subsequent work. (4) The broad range of unique environments of lunar PSRs, especially the cold temperatures, would invariably introduce peculiar surface modification mechanisms, including impact comminution and gardening, physical and chemical weathering, and mass movements; their potential effects on the observed LOLA 1,064-nm albedo should be quantified through experimental and/or theoretical investigations in future studies. (5) Our crater population investigation of the Amundsen crater floor shows that the PSR have fewer smaller (<800 m) superposed impact craters than the adjacent non-PSR (section 3.2). The decreased small crater density will reduce the small-scale roughness of the local surface, which, potentially, may increase the observed LOLA albedo. To interpret the elevated LOLA reflectance of lunar PSRs unambiguously, the effect of surface roughness on LOLA reflectance also requires further examination. (6) Volatile species other than water have been directly detected in the ejecta plume from the Cabeus floor PSR (Gladstone et al., 2012; Schultz et al., 2010) and are thought to be present in many more lunar PSRs (Fisher et al., 2017). On Mercury, these volatile species have been observed to exhibit very different and complicated optical reflectance behaviors than water ice; in particular, some volatiles (e.g., carbon-bearing species and organics) are characterized by apparently lower reflectance than the background (Chabot et al., 2014; Deutsch et al., 2017; Neumann et al., 2013). The involvement of these volatiles would make the water ice detection and characterization based on LOLA reflectivity measurements more challenging, which deserves further explorations.

In addition, while our investigations mainly focus on LOLA surface reflectivity measurements, our analysis strategy of targeting the very flat PSRs and comparing these with the immediately adjacent similarly flat non-PSRs also apply to other data-based water ice detections. Remote sensing measurements of a wide range of electromagnetic wavelengths, in addition to the near-infrared wavelength covered by LOLA, are often subject to slope and its related effects. For instance, local observational incidence angle differences induced by topographic slopes have been shown to result in significant discrepancies among radar backscattering

measurements (e.g., Fa & Cai, 2013). Examining electromagnetic measurements of these flat PSRs at radar and other wavelengths should adequately exclude slope and the related effects outlined here.

6. Reference Analysis for Future Surface In Situ Exploration

Water ice and other enhancements of volatiles in PSRs has become a burgeoning subfield of lunar and planetary science, particularly for Mercury (e.g., Deutsch et al., 2016) and the Moon and one of the most prioritized exploration targets for previous and future lunar missions. Over the last decade, multiple nations have described extensive visions, plans, and proposed missions for lunar polar exploration. In the near future, we will likely have abundant missions targeting and studying lunar PSR candidate water ice locations (orbital, landed, and human sortie; e.g., https://lunarvolatiles.nasa.gov/current-activities). Many fundamental knowledge gaps for lunar PSRs and PSR water ice, for example, compositional state and distribution, source(s), and migration processes (National Research Council, 2007), will require surface in situ measurements from landed missions within PSRs (e.g., Lawrence, 2017). Our investigation of the surface water ice detection and characterization on the basis of LOLA reflectivity measurements can provide an important reference base for future PSR water ice-specific missions in various aspects, including landing and sampling site selection and surface operations strategy planning.

Previous water ice investigations in specific polar PSRs has usually focused on several large craters in the south polar regions, for example, Shackleton at the south pole, Haworth, Shoemaker, Faustini, and Cabeus (e.g., Gladstone et al., 2012; Hayne et al., 2015; Lucey et al., 2014; Zuber et al., 2012). These large craters are the most prominent geomorphologic features whose entire interior floors are permanently shadowed in the immediate surroundings of the lunar south pole. These craters also host the most areally extensive PSRs on the Moon; for instance, the Shoemaker and Haworth interior PSRs both have surface areas of over 1,000 km^2. Prior studies have provided multiple lines of evidences for hydrogen/water ice concentrations within these large craters (e.g., Boynton et al., 2012; Hayne et al., 2015; Gladstone et al., 2012; Litvak et al., 2012; Li et al., 2018; Sanin et al., 2017), making these craters science-rich candidate landing sites for future lunar surface water prospector missions (e.g., Flahaut et al., 2016; Neal & Lawrence, 2017). Our focused water ice detection and characterization investigation in polar crater flat floors (with a combination of PSRs and non-PSRs) provides an alternative perspective on the selection of optimal landing sites. The focus on the flat and part-PSR polar crater floors has advantages in the following aspects of scientific and exploration objectives: (1) restricting working areas within very flat surfaces can convincingly eliminate the potential effect of topographic slope on the inferred water ice presence from surface reflectivity measurements; (2) the involvement of the immediately adjacent non-PSRs serve as an excellent control group, and the comparative analysis of the LOLA albedo of PSRs and their adjacent non-PSRs can adequately eliminate the potential uncertainty from the compositional heterogeneous of lunar polar crust, and thus optimize the detection of the reflectivity anomalies of these analyzed PSRs; (3) the very flat terrain of our PSRs studied can definitely facilitate surface exploration activities, including controlled soft-landing, rover navigability and mobility, and surface operations and experiments; and (4) the adjacent non-PSRs may provide additional exploration strategy possibilities; for example, direct landing on the PSRs, requiring dealing with the harsh cold temperature and the lack of solar illumination for navigation and power, is much more challenging than landing on non-PSRs and then roving into the immediately adjacent PSRs. Our investigation proposes these polar PSR-hosting craters with relatively extensive flat floors as high-priority landing sites and exploration targets, especially the Amundsen crater in the southern polar region and the Lovelace crater in the north polar region. Our recommendation of the Amundsen crater is exactly in line with the recommendations of Kring and Durda (2012) and Lemelin et al. (2014).

The Amundsen crater is 103 km in diameter and located ~170 km from the south pole (centered at 83.07°E, 84.44°S), within the South Pole-Aitken basin. Amundsen is a typical lunar complex crater, with a well-developed continuous ejecta deposit and wall terraces. This crater hosts a very extensive (67 × 60-km size) and flat (mean 60-m baseline slope of 5.3 ± 5.0°) floor terrain (Figure 11), which is easily sufficient to accommodate a landing ellipse for a landed mission, for example, a 15 × 30-km landing ellipse for the Russia Luna-Glob mission (Djachkova et al., 2017; Ivanov et al., 2018). Previous stratigraphic analysis of Apollo orbital photographs has assigned this crater to the Nectarian system (Wilhelms et al., 1987; Wilhelms & Byrne, 2009), and our crater population investigation of the crater flat floor suggests a comparable or slightly older

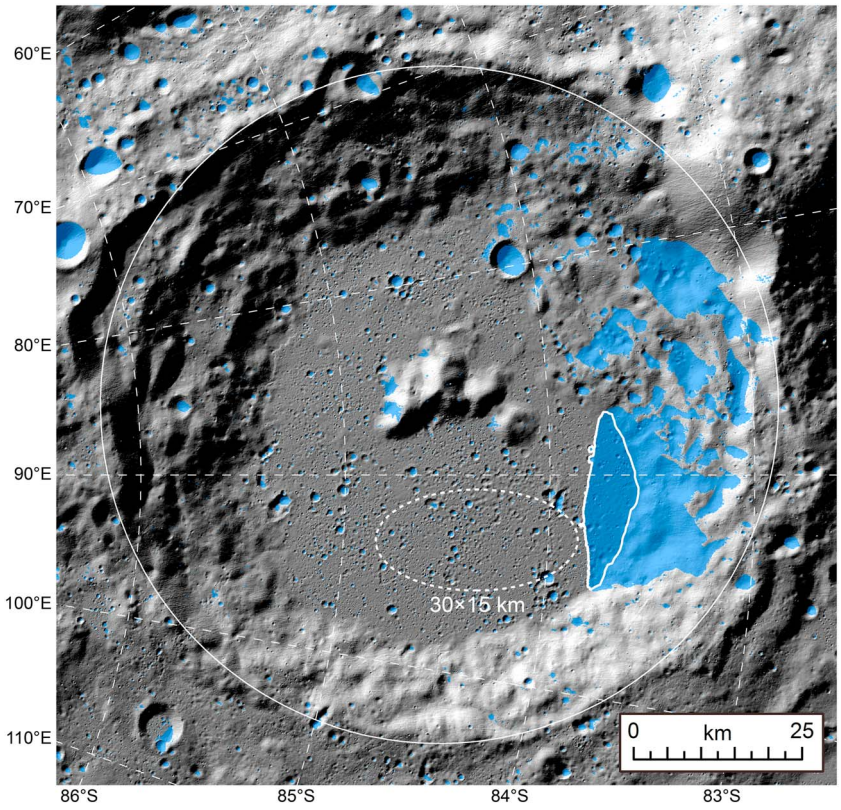


Figure 11. Amundsen crater: Lunar Orbiter Laser Altimeter topography-derived shaded relief map (315° azimuth angle and 10° altitude angle). The thin white circle is the rim crest position of Amundsen from Head et al. (2010), the blue patchy areas are the permanently shadowed regions mapped out by Mazarico et al. (2011), the bold white polygon outlines the 132-km^2 flat permanently shadowed regions in the north floor edge, and the dashed ellipse marks a 30 × 15 landing ellipse.

age, ~4.0 Ga in the pre-Nectarian system. A central peak structure with a size of 25 × 16 km is observed in the central floor. This central peak structure is composed of four major peaks, arranged in an arcuate pattern, resembling those observed in the so-called ringed peak-cluster craters, for example, the 84-km-diameter Metius crater (Baker et al., 2011). The heights of these central peaks from the floor range from 0.62 to 1.2 km.

Numerous PSRs occur in the crater interior, ranging from micro-PSRs <1 km^2 within small depressions on the floor and areally extensive, ~375-km^2 PSR on the north wall (Figure 11). The north marginal crater floor hosts the second largest flat floor PSR on the Moon (only the Sverdrup floor PSR is larger), which has a size of 26 × 8 km and a surface area of 132 km^2 (Figure 11). Such a flat and extensive floor terrain would be readily accessible for a landed and/or roving mission. Hydrogen concentration measured by Lunar Prospector neutron spectrometer revealed an elevated hydrogen abundance of over 100 ppm (Feldman et al., 2001), and LRO Lyman Alpha Mapping Project ultraviolet albedo measurements identified numerous locations within this PSR with ultraviolet spectra consistent with exposed water ice (Hayne et al., 2015). Our LOLA 1,064-nm albedo characterization shows that this PSR is ~10% more reflective than the adjacent flat non-PSR. Simple linear albedo unmixing yields a model water ice content of ~6% for the Amundsen PSR, whereas intimate unmixing calculation with the consideration of a medium porosity effect gives an even higher, ~12% model water ice abundance (section 5.2). Lemelin et al. (2014) have presented a thorough case study of Amundsen crater as an optimized exploration target for landing site, sample locations, and exploration strategies.

7. Conclusions

On the basis of our detailed LOLA albedo data-based water ice detection and characterization in all major PSRs in lunar polar crater flat floors presented above, we draw the following conclusions:

1. The vast majority (71 of 75) of all analyzed PSRs in both polar regions are systematically more reflective at 1,064 nm than their adjacent non-PSR regions, with an average positive anomaly of ~5%. Several ($n = 9$) PSRs have albedo values more than 10% higher than the surrounding areas; these specific higher water concentrations serve as the most promising water ice-hosting PSRs on the Moon.
2. Various factors including solar illumination, surface temperature, composition variations, boulder exposure, topographic slopes and their related effects on space weathering, physical disruption, and mass motion cannot solely explain the observed LOLA albedo anomalies of the studied PSRs; we conclude that exposed surface water ice serves as the most plausible explanation.
3. Surface water ice exposure is suggested to be a prevalent behavior for major cold trap regions on the Moon. However, the inferred exposed water ice shows lateral heterogeneity in model ice abundances, ranging from negligible to ~6% by area, consistent with previous LCROSS ground truth measurements (Colaprete et al., 2010) and LRO Lyman Alpha Mapping Project ultraviolet albedo measurements (Hayne et al., 2015). This spatial composition distribution may indicate differential water delivery flux and/or loss rates.
4. Impact crater population and depth measurements show that the interpreted surface water ice exposures are small in total thickness and abundance, consistent with radar echo observations. PSRs water ice may be in the form of surface frost layers or admixtures of water ice particles with lunar regolith, suggesting that possible dynamic retention and sublimation processes are important in lunar polar water ice occurrences.
5. We propose that the flat crater floor PSRs studied serve as optimal landing targets for future surface in situ exploration endeavors and that they hold both significant scientific promise and engineering feasibility. In particular, the Amundsen crater PSR is suggested to be a high-priority landing and exploration site, in line with previous recommendations (Kring & Durda, 2012; Lemelin et al., 2014).

Acknowledgments
L. Q. acknowledges Hui Liu for advices on the null hypothesis tests, Jay Dickson for assistances on LOLA albedo data acquisition and processing, and Yazhou Yang for help on single scattering albedo unmixing calculation and water ice content estimations. This work is partly supported by the Key Research Program of the Chinese Academy of Sciences (Grant XDPB11), the Open Fund of State Key Laboratory of Remote Sensing Science (Grant OFSLRSS201807), China Postdoctoral Science Foundation (2018T110682 and 2017M610421), the National Natural Science Foundation of China (41703063 and 41473065), and Shandong Natural Science Foundation (JQ201511). We gratefully acknowledge financial support by Russian Science Foundation grant 17-17-01149 to M. A. I. All original LRO data can be found in the NASA's Planetary Data System (http://pds.nasa.gov/), and the original Kaguya/SELENE Multiband Imager data are archived at SELENE Data Archive (https://darts.isas.jaxa.jp/planet/pdap/selene/).

References

Baker, D. M. H., Head, J. W., Fassett, C. I., Kadish, S. J., Smith, D. E., Zuber, M. T., & Neumann, G. A. (2011). The transition from complex crater to peak-ring basin on the Moon: New observations from the Lunar Orbiter Laser Altimeter (LOLA) instrument. *Icarus*, *214*(2), 377–393. https://doi.org/10.1016/j.icarus.2011.05.030

Basilevsky, A. T. (1976). On the evolution rate of small craters. *Proceedings of the Lunar Science Conference*, *7*, 1005–1020.

Basilevsky, A. T., Head, J. W., & Horz, F. (2013). Survival times of meter-sized boulders on the surface of the Moon. *Planetary and Space Science*, *89*, 118–126. https://doi.org/10.1016/j.pss.2013.07.011

Boynton, W. V., Droege, G. F., Mitrofanov, I. G., McClanahan, T. P., Sanin, A. B., Litvak, M. L., et al. (2012). High spatial resolution studies of epithermal neutron emission from the lunar poles: Constraints on hydrogen mobility. *Journal of Geophysical Research*, *117*, E00H33. https://doi.org/10.1029/2011JE003979

Brandt, R. E., Warren, S. G., Worby, A. P., & Grenfell, T. C. (2005). Surface albedo of the Antarctic sea ice zone. *Journal of Climate*, *18*(17), 3606–3622.

Cahill, J. T. S., Lucey, P. G., & Wieczorek, M. A. (2009). Compositional variations of the lunar crust: Results from radiative transfer modeling of central peak spectra. *Journal of Geophysical Research*, *114*, E09001. https://doi.org/10.1029/2008JE003282

Campbell, D. B., Campbell, B. A., Carter, L. M., Margot, J.-L., & Stacy, N. J. S. (2006). No evidence for thick deposits of ice at the lunar south pole. *Nature*, *443*, 835. https://doi.org/10.1038/nature05167

Chabot, N. L., Ernst, C. M., Denevi, B. W., Nair, H., Deutsch, A. N., Blewett, D. T., et al. (2014). Images of surface volatiles in Mercury's polar craters acquired by the MESSENGER spacecraft. *Geology*, *42*(12), 1051–1054. https://doi.org/10.1130/g35916.1

Cisneros, E., Awumah, A., Brown, H. M., Martin, A. C., Paris, K. N., Povilaitis, R. Z., et al. (2017). Lunar Reconnaissance Orbiter Camera permanently shadowed region imaging—Atlas and controlled mosaics. *48th Lunar and Planetary Science Conference*, Lunar and Planetary Institute, The Woodlands, Texas, abstract #2469.

Colaprete, A., Schultz, P., Heldmann, J., Wooden, D., Shirley, M., Ennico, K., et al. (2010). Detection of water in the LCROSS ejecta plume. *Science*, *330*(6003), 463–468. https://doi.org/10.1126/science.1186986

Corley, L. M., Gillis-Davis, J. J., Lucey, P. G., & Trang, D. (2016). Space weathering at the lunar poles: the effect of temperature on reflectance of materials weathered by laser irradiation. *47th Lunar and Planetary Science Conference*, Lunar and Planetary Institute, The Woodlands, Texas, abstract #2692.

Corley, L. M., Gillis-Davis, J. J., Lucey, P. G., & Trang, D. (2017). The Effect of temperature on the reflectance spectra of pyroxene and a highlands analog weathered by laser irradiation. *48th Lunar and Planetary Science Conference*, Lunar and Planetary Institute, The Woodlands, Texas, abstract #1698.

Deutsch, A. N., Chabot, N. L., Mazarico, E., Ernst, C. M., Head, J. W., Neumann, G. A., & Solomon, S. C. (2016). Comparison of areas in shadow from imaging and altimetry in the north polar region of Mercury and implications for polar ice deposits. *Icarus*, *280*, 158–171. https://doi.org/10.1016/j.icarus.2016.06.015

Deutsch, A. N., Head, J. W., Chabot, N. L., & Neumann, G. A. (2018). Constraining the thickness of polar ice deposits on Mercury using the Mercury Laser Altimeter and small craters in permanently shadowed regions. *Icarus*, *305*, 139–148. https://doi.org/10.1016/j.icarus.2018.01.013

Deutsch, A. N., Neumann, G. A., & Head, J. W. (2017). New evidence for surface water ice in small-scale cold traps and in three large craters at the north polar region of Mercury from the Mercury Laser Altimeter. *Geophysical Research Letters*, *44*, 9233–9241. https://doi.org/10.1002/2017GL074723

Djachkova, M. V., Litvak, M. L., Mitrofanov, I. G., & Sanin, A. B. (2017). Selection of Luna-25 landing sites in the south polar region of the moon. *Solar System Research*, *51*(3), 185–195. https://doi.org/10.1134/S0038094617030029

Donaldson Hanna, K. L. D., Cheek, L. C., Pieters, C. M., Mustard, J. F., Greenhagen, B. T., Thomas, I. R., & Bowles, N. E. (2014). Global assessment of pure crystalline plagioclase across the Moon and implications for the evolution of the primary crust. *Journal of Geophysical Research: Planets*, *119*, 1516–1545. https://doi.org/10.1002/2013JE004476

Eke, V. R., Lawrence, D. J., & Teodoro, L. F. A. (2017). How thick are Mercury's polar water ice deposits? *Icarus*, *284*, 407–415. https://doi.org/10.1016/j.icarus.2016.12.001

Fa, W., & Cai, Y. (2013). Circular polarization ratio characteristics of impact craters from Mini-RF observations and implications for ice detection at the polar regions of the Moon. *Journal of Geophysical Research: Planets*, *118*, 1582–1608. https://doi.org/10.1002/jgre.20110

Farrell, W. M., Stubbs, T. J., Halekas, J. S., Killen, R. M., Delory, G. T., Collier, M. R., & Vondrak, R. R. (2010). Anticipated electrical environment within permanently shadowed lunar craters. *Journal of Geophysical Research*, *115*, E03004. https://doi.org/10.1029/2009JE003464

Fassett, C. I. (2016). Analysis of impact crater populations and the geochronology of planetary surfaces in the inner solar system. *Journal of Geophysical Research: Planets*, *121*, 1900–1926. https://doi.org/10.1002/2016JE005094

Feldman, W. C., Maurice, S., Lawrence, D. J., Little, R. C., Lawson, S. L., Gasnault, O., et al. (2001). Evidence for water ice near the lunar poles. *Journal of Geophysical Research*, *106*, 23,231–23,251. https://doi.org/10.1029/2000JE001444

Fisher, E. A., Lucey, P. G., Lemelin, M., Greenhagen, B. T., Siegler, M. A., Mazarico, E., et al. (2017). Evidence for surface water ice in the lunar polar regions using reflectance measurements from the Lunar Orbiter Laser Altimeter and temperature measurements from the Diviner Lunar Radiometer Experiment. *Icarus*, *292*, 74–85. https://doi.org/10.1016/j.icarus.2017.03.023

Flahaut, J., Carpenter, J., Anand, M., van Westrenen, W., Fisackerly, R., Williams, J.-P., et al., & ESA Topical Team on the Exploitation of Local Planetary Material (2016). Candidate landing sites near the lunar poles: A European perspective. 4th *European Lunar Symposium*, Dutch Royal Academy of Arts and Sciences, Amsterdam, The Netherlands, abstract #004.

Gladstone, G. R., Retherford, K. D., Egan, A. F., Kaufmann, D. E., Miles, P. F., Parker, J. W., et al. (2012). Far-ultraviolet reflectance properties of the Moon's permanently shadowed regions. *Journal of Geophysical Research*, *117*, E00H04. https://doi.org/10.1029/2011JE003913

Hapke, B. (1990). Coherent backscatter and the radar characteristics of outer planet satellites. *Icarus*, *88*(2), 407–417. https://doi.org/10.1016/0019-1035(90)90091-m

Hapke, B. (1993). *Theory of Reflectance and Emittance Spectroscopy*. Cambridge: Cambridge University Press.

Hapke, B. (2008). Bidirectional reflectance spectroscopy: 6. Effects of porosity. *Icarus*, *195*(2), 918–926. https://doi.org/10.1016/j.icarus.2008.01.003

Haruyama, J., Ohtake, M., Matsunaga, T., Morota, T., Honda, C., Yokota, Y., et al. (2008). Lack of exposed ice inside lunar south pole Shackleton crater. *Science*, *322*(5903), 938–939. https://doi.org/10.1126/science.1164020

Haruyama, J., Yamamoto, S., Yokota, Y., Ohtake, M., & Matsunaga, T. (2013). An explanation of bright areas inside Shackleton Crater at the lunar south pole other than water-ice deposits. *Geophysical Research Letters*, *40*, 3814–3818. https://doi.org/10.1002/grl.50753

Hayne, P. O., Greenhagen, B. T., Foote, M. C., Siegler, M. A., Vasavada, A. R., & Paige, D. A. (2010). Diviner lunar radiometer observations of the LCROSS impact. *Science*, *330*(6003), 477–479. https://doi.org/10.1126/science.1197135

Hayne, P. O., Hendrix, A., Sefton-Nash, E., Siegler, M. A., Lucey, P. G., Retherford, K. D., et al. (2015). Evidence for exposed water ice in the Moon's south polar regions from Lunar Reconnaissance Orbiter ultraviolet albedo and temperature measurements. *Icarus*, *255*, 58–69. https://doi.org/10.1016/j.icarus.2015.03.032

Head, J. W. III, Fassett, C. I., Kadish, S. J., Smith, D. E., Zuber, M. T., Neumann, G. A., & Mazarico, E. (2010). Global distribution of large lunar craters: Implications for resurfacing and impactor populations. *Science*, *329*(5998), 1504–1507. https://doi.org/10.1126/science.1195050

Head, J. W., & Wilson, L. (2017). Generation, ascent and eruption of magma on the Moon: New insights into source depths, magma supply, intrusions and effusive/explosive eruptions (Part 2: Predicted emplacement processes and observations). *Icarus*, *283*, 176–223. https://doi.org/10.1016/j.icarus.2016.05.031

Hemingway, D. J., Garrick-Bethell, I., & Kreslavsky, M. A. (2015). Latitudinal variation in spectral properties of the lunar maria and implications for space weathering. *Icarus*, *261*, 66–79. https://doi.org/10.1016/j.icarus.2015.08.004

Ivanov, M. A., Abdrakhimov, A. M., Basilevsky, A. T., Demidov, N. E., Guseva, E. N., Head, J. W., et al. (2018). Geological characterization of the three high-priority landing sites for the Luna-Glob mission. *Planetary and Space Science*, *162*, 190–206. https://doi.org/10.1016/j.pss.2017.08.004

Koeber, S. D., & Robinson, M. S. (2013). LROC observations of permanently shadowed regions. *44th Lunar and Planetary Science Conference*, Lunar and Planetary Institute, The Woodlands, Texas, abstract #2588.

Kring, D. A., & Durda, D. D. (Eds.) (2012). *A global lunar landing site study to provide the scientific context for exploration of the Moon*. Houston, TX: Lunar and Planetary Institute.

Krishna, N., & Kumar, P. S. (2016). Impact spallation processes on the Moon: A case study from the size and shape analysis of ejecta boulders and secondary craters of Censorinus crater. *Icarus*, *264*(Supplement C, 274–299. https://doi.org/10.1016/j.icarus.2015.09.033

Lawrence, D. J. (2017). A tale of two poles: Toward understanding the presence, distribution, and origin of volatiles at the polar regions of the Moon and Mercury. *Journal of Geophysical Research: Planets*, *122*, 21–52. https://doi.org/10.1002/2016JE005167

Lemelin, M., Blair, D. M., Roberts, C. E., Runyon, K. D., Nowka, D., & Kring, D. A. (2014). High-priority lunar landing sites for in situ and sample return studies of polar volatiles. *Planetary and Space Science*, *101*, 149–161. https://doi.org/10.1016/j.pss.2014.07.002

Lemelin, M., Lucey, P. G., Neumann, G. A., Mazarico, E. M., Barker, M. K., Kakazu, A., et al. (2016). Improved calibration of reflectance data from the LRO Lunar Orbiter Laser Altimeter (LOLA) and implications for space weathering. *Icarus*, *273*, 315–328. https://doi.org/10.1016/j.icarus.2016.02.006

Li, S., Lucey, P. G., Milliken, R. E., Hayne, P. O., Fisher, E., Williams, J.-P., et al. (2018). Direct evidence of surface exposed water ice in the lunar polar regions. *Proceedings of the National Academy of Sciences*, *115*(36), 8907–8912.. https://doi.org/10.1073/pnas.1802345115

Litvak, M. L., Mitrofanov, I. G., Sanin, A., Malakhov, A., Boynton, W. V., Chin, G., et al. (2012). Global maps of lunar neutron fluxes from the LEND instrument. *Journal of Geophysical Research*, *117*, E00H22. https://doi.org/10.1029/2011JE003949

Lucey, P. G., Neumann, G. A., Riner, M. A., Mazarico, E., Smith, D. E., Zuber, M. T., et al. (2014). The global albedo of the Moon at 1064 nm from LOLA. *Journal of Geophysical Research: Planets*, *119*, 1665–1679. https://doi.org/10.1002/2013JE004592

Mazarico, E., Neumann, G. A., Smith, D. E., Zuber, M. T., & Torrence, M. H. (2011). Illumination conditions of the lunar polar regions using LOLA topography. *Icarus*, *211*(2), 1066–1081. https://doi.org/10.1016/j.icarus.2010.10.030

Michael, G. G., Kneissl, T., & Neesemann, A. (2016). Planetary surface dating from crater size-frequency distribution measurements: Poisson timing analysis. *Icarus*, *277*, 279–285. https://doi.org/10.1016/j.icarus.2016.05.019

Michael, G. G., & Neukum, G. (2010). Planetary surface dating from crater size-frequency distribution measurements: Partial resurfacing events and statistical age uncertainty. *Earth and Planetary Science Letters*, *294*(3-4), 223–229. https://doi.org/10.1016/j.epsl.2009.12.041

Mitchell, J., Lawrence, S., Robinson, M., Speyerer, E., & Denevi, B. (2017). Using complementary remote sensing techniques to assess the presence of volatiles at the lunar north pole. *Planetary and Space Science*. https://doi.org/10.1016/j.pss.2017.07.015

National Research Council (2007). *The scientific context for exploration of the Moon*. Washington, DC: National Academies Press.

Neal, C. R., & Lawrence, S. J. (2017). A multi-decadal sample return campaign will advance lunar and solar system science and exploration by 2050. *Planetary Science Vision 2050 Workshop*, NASA headquarters, Washington, DC, abstract #8142.

Needham, D. H., & Kring, D. A. (2017). Lunar volcanism produced a transient atmosphere around the ancient Moon. *Earth and Planetary Science Letters*, *478*, 175–178. https://doi.org/10.1016/j.epsl.2017.09.002

Neukum, G., Ivanov, B. A., & Hartmann, W. K. (2001). Cratering records in the inner solar system in relation to the lunar reference system. *Space Science Reviews*, *96*(1-4), 55–86. https://doi.org/10.1023/A:1011989004263

Neumann, G. A., Cavanaugh, J. F., Sun, X., Mazarico, E. M., Smith, D. E., Zuber, M. T., et al. (2013). Bright and dark polar deposits on Mercury: Evidence for surface volatiles. *Science*, *339*(6117), 296–300. https://doi.org/10.1126/science.1229764

Nozette, S., Spudis, P., Bussey, B., Jensen, R., Raney, K., Winters, H., et al. (2010). The Lunar Reconnaissance Orbiter Miniature Radio Frequency (Mini-RF) technology demonstration. *Space Science Reviews*, *150*(1-4), 285–302. https://doi.org/10.1007/s11214-009-9607-5

Oberbeck, V., & Morrison, R. (1974). Laboratory simulation of the herringbone pattern associated with lunar secondary crater chains. *The Moon*, *9*(3-4), 415–455.

Ohtake, M., Haruyama, J., Matsunaga, T., Yokota, Y., Morota, T., Honda, C., & team, L. (2008). Performance and scientific objectives of the SELENE (KAGUYA) Multiband Imager. *Earth, Planets and Space*, *60*(4), 257–264. https://doi.org/10.1186/BF03352789

Ohtake, M., Takeda, H., Matsunaga, T., Yokota, Y., Haruyama, J., Morota, T., et al. (2012). Asymmetric crustal growth on the Moon indicated by primitive farside highland materials. *Nature Geoscience*, *5*(6), 384. https://doi.org/10.1038/ngeo1458–388.

Paige, D. A., Siegler, M. A., Zhang, J. A., Hayne, P. O., Foote, E. J., Bennett, K. A., et al. (2010). Diviner lunar radiometer observations of cold traps in the Moon's south polar region. *Science*, *330*(6003), 479–482. https://doi.org/10.1126/science.1187726

Pieters, C. M., & Noble, S. K. (2016). Space weathering on airless bodies. *Journal of Geophysical Research: Planets*, *121*, 1865–1884. https://doi.org/10.1002/2016JE005128

Qiao, L., Head, J. W., Xiao, L., Wilson, L., & Dufek, J. D. (2018). The role of substrate characteristics in producing anomalously young crater retention ages in volcanic deposits on the Moon: Morphology, topography, subresolution roughness, and mode of emplacement of the Sosigenes lunar irregular mare patch. *Meteoritics & Planetary Science*, *53*(4), 778–812. https://doi.org/10.1111/maps.13003

Raney, R. K., Cahill, J. T. S., Patterson, G. W., & Bussey, D. B. J. (2012). The *m-chi* decomposition of hybrid dual-polarimetric radar data with application to lunar craters. *Journal of Geophysical Research*, *117*, E00H21. https://doi.org/10.1029/2011JE003986

Robinson, M. S., Mahanti, P., Carter, L. M., Denevi, B. W., Estes, N. M., Ravine, M. A., et al. (2017). ShadowCam—Seeing in the dark. *European Planetary Science Congress 2017*, Riga, Latvia, vol. 11, abstract #EPSC2017-506.

Sanin, A. B., Mitrofanov, I. G., Litvak, M. L., Bakhtin, B. N., Bodnarik, J. G., Boynton, W. V., et al. (2017). Hydrogen distribution in the lunar polar regions. *Icarus*, *283*, 20–30. https://doi.org/10.1016/j.icarus.2016.06.002

Schorghofer, N., & Taylor, G. J. (2007). Subsurface migration of H_2O at lunar cold traps. *Journal of Geophysical Research*, *112*, E02010. https://doi.org/10.1029/2006JE002779

Schultz, P. H., Hermalyn, B., Colaprete, A., Ennico, K., Shirley, M., & Marshall, W. S. (2010). The LCROSS cratering experiment. *Science*, *330*(6003), 468–472. https://doi.org/10.1126/science.1187454

Shoemaker, E. M. (1962). Interpretation of lunar craters. In Z. Kopal (Ed.), *Physics and astronomy of the Moon* (pp. 283–360). New York: Academic Press.

Siegler, M., Paige, D., Williams, J.-P., & Bills, B. (2015). Evolution of lunar polar ice stability. *Icarus*, *255*, 78–87. https://doi.org/10.1016/j.icarus.2014.09.037

Siegler, M. A., Miller, R. S., Keane, J. T., Laneuville, M., Paige, D. A., Matsuyama, I., et al. (2016). Lunar true polar wander inferred from polar hydrogen. *Nature*, *531*(7595), 480–484. https://doi.org/10.1038/nature17166

Sim, C. K., Kim, S. S., Lucey, P. G., Garrick-Bethell, I., & Choi, Y. J. (2017). Asymmetric space weathering on lunar crater walls. *Geophysical Research Letters*, *44*, 11,273–211,281. https://doi.org/10.1002/2017GL075338

Smith, D. E., Zuber, M. T., Jackson, G. B., Cavanaugh, J. F., Neumann, G. A., Riris, H., et al. (2010). The Lunar Orbiter Laser Altimeter investigation on the Lunar Reconnaissance Orbiter mission. *Space Science Reviews*, *150*(1-4), 209–241. https://doi.org/10.1007/s11214-009-9512-y

Smith, D. E., Zuber, M. T., Neumann, G. A., Mazarico, E., Lemoine, F. G., Head, J. W. III, et al. (2017). Summary of the results from the lunar orbiter laser altimeter after seven years in lunar orbit. *Icarus*, *283*, 70–91. https://doi.org/10.1016/j.icarus.2016.06.006

Speyerer, E. J., & Robinson, M. S. (2013). Persistently illuminated regions at the lunar poles: Ideal sites for future exploration. *Icarus*, *222*(1), 122–136. https://doi.org/10.1016/j.icarus.2012.10.010

Trask, N. J. (1966). Size and spatial distribution of craters estimated from the Ranger photographs. In *Ranger VIII and IX, Part II, Experimenters' analyses and interpretations* (Technical Reports 32-800, (pp. 252–264). Pasadena, CA: Jet Propulsion Laboratory.

Tye, A. R., Fassett, C. I., Head, J. W., Mazarico, E., Basilevsky, A. T., Neumann, G. A., et al. (2015). The age of lunar south circumpolar craters Haworth, Shoemaker, Faustini, and Shackleton: Implications for regional geology, surface processes, and volatile sequestration. *Icarus*, *255*, 70–77. https://doi.org/10.1016/j.icarus.2015.03.016

Watson, K., Murray, B., & Brown, H. (1961). On the possible presence of ice on the Moon. *Journal of Geophysical Research*, *66*(5), 1598–1600.

Wilhelms, D. E., & Byrne, C. J. (2009). Stratigraphy of lunar craters, *Image again online*: http://www.imageagain.com/Strata/StratigraphyCraters.2.0.htm.

Wilhelms, D. E., McCauley, J. F., & Trask, N. J. (1987). *The geologic history of the Moon*, *U.S. Geological Survey Professional Paper 1348*, (p. 302). Washington: United States Government Printing Office.

Xiao, Z., Zeng, Z., Ding, N., & Molaro, J. (2013). Mass wasting features on the Moon-how active is the lunar surface? *Earth and Planetary Science Letters*, *376*, 1–11. https://doi.org/10.1016/j.epsl.2013.06.015

Yamamoto, S., Nakamura, R., Matsunaga, T., Ogawa, Y., Ishihara, Y., Morota, T., et al. (2012). Massive layer of pure anorthosite on the Moon. *Geophysical Research Letters*, *39*, L13201. https://doi.org/10.1029/2012GL052098

Zhang, J. A., & Paige, D. A. (2009). Cold-trapped organic compounds at the poles of the Moon and Mercury: Implications for origins. *Geophysical Research Letters*, *36*, L16203. https://doi.org/10.1029/2009GL038614

Zuber, M. T., Head, J. W., Smith, D. E., Neumann, G. A., Mazarico, E., Torrence, M. H., et al. (2012). Constraints on the volatile distribution within Shackleton crater at the lunar south pole. *Nature*, *486*(7403), 378–381. https://doi.org/10.1038/nature11216